This is to certify that the

thesis entitled

Fluorescent Thermography Methods for Bio-Thermal Therapies

presented by

Damien J. Fron

has been accepted towards fulfillment
of the requirements for

MS degree in Mechanical Engineering

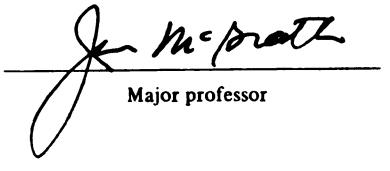

Major professor

Date 8/14/02

FLUORESCENT THERMOGRAPHY METHODS FOR BIO-THERMAL THERAPIES

By

Damien J. Fron

A THESIS

Submitted to
Michigan State University
in partial fulfillment of the requirements
for the degree of

MASTERS OF SCIENCE

Department of Mechanical Engineering

2002

ABSTRACT

FLUORESCENT THERMOGRAPHY METHODS FOR BIO-THERMAL THERAPIES

By

Damien J. Fron

Thermotherapy by way of laser and radiofrequency (RF) heating devices has become ever more popular for the treatment of joint instabilities associated with the knee, shoulder, wrist, and hip. Similarly, cooling/freezing therapies are of biomedical interest at the opposite temperature extreme for such applications as cryosurgical ablation of tumors. This thesis addresses the need for improved methods of temperature measurement required to understand the performance of various thermotherapy devices as well as the thermal response they produce within biomaterials. Two fluorescent thermography methods of biomedical interest have been developed to measure temperatures from –80°C to +90°C using temperature-dependent fluorescent techniques. Temperatures as high as 90°C were recorded within aqueous solutions and tissue phantoms using two-color laser-induced fluorescence thermography (LIFT) and the ratio of the fluorescent emission intensities of the dissolved fluorescent dyes Rhodamine B and Rhodamine 110. The feasibility of using fluorescent chemicals to measure temperatures for cryogenic application was evaluated using fluorescent emission ratiometric imaging thermography (FERIT) and the fluorescent emission intensity of Terbium. Present capabilities of the fluorescent thermography methods mentioned enable 10 Hz framing rates at an accuracy of 1.5°C, with a spatial resolution of 90 μm and a temperature resolution of 0.02°C.

ACKNOWLEDGEMENTS

I would like to take a few moments to thank those who have supported me throughout my graduate career at Michigan State University. First, I would like to thank my advisor Dr. John J. McGrath. He welcomed me into his lab as an undergraduate assistant for his graduate students, and because of those experiences and his encouragement, I eventually decided to pursue my masters degree with him. I believe that many of my experiences in his labs have turned me into the student I am today. Dr. McGrath exhibits excellent commitment to his students and has been a positive role model in my life. I thank him for all that he has taught me these past few years.

I would also like to thank my guidance committee members Dr. Neil Wright and Dr. Robert McMasters for their comments and advice on my thesis. The time you spent with me helped me to explore the full scope of my project.

In the three years I worked in Dr. McGrath's lab I had the pleasure of knowing Dr. Gloria Elliott, Dr. Paul Hoke, and Dr. Alptekin Aksan. One by one they graduated leaving me by myself under the full attention of Dr. McGrath. I thank them for their friendship and for sharing their knowledge and experiences with me. A special thanks to Dr. Aksan who taught me: "A day in the lab without disrespect is not a day in the lab."

In addition to those already mentioned I appreciate the many hours of advice and discussion from Nate Verhanovitz and Chee Lum. Thank you for your help since it surely contributed to the completion of this thesis.

I am also thankful to my mom, dad, and brother for their enduring support throughout the years. I know they thought I would never be done and I could not have finished without their love. Just think, I could have continued for my Ph.D. Last and surely not least I thank my love, Sara, who saw me through the ups and downs of my graduate career and offered endless encouragement and compassion.

TABLE OF CONTENTS

LIST OF TABLES vii

LIST OF FIGURES viii

KEY TO SYMBOLS AND ABBREVIATIONS xi

Chapter 1: Introduction 1
1.1 Introduction to Radiofrequency Heating 3
1.2 Evaluation of Common Temperature Measurement Techniques 5
1.2.1 Thermocouples 5
1.2.2 Fluoroptic Thermometry 7
1.2.3 Infrared Thermography 8
1.3 Introduction to Temperature Measurement at Cryogenic Levels 11
1.4 Fundamentals of Luminescence 12
1.5 Theory of Temperature Dependent Fluorescence 16
1.6 Introduction to LIFT 18
1.7 Introduction to FERIT 20

Chapter 2: Evaluation of Temperature Dependent Fluorescent Chemicals 22
2.1 Evaluation of Fluorophores with a Spectrometer 24
2.2 Evaluation of the FERIT Fluorescent Chemicals 28
2.3 Spectral Evaluation of the Polymer Based Fluorophores with the Ocean Optics Spectrometer 29
2.4 FERIT Ratiometric Methods for the Determination of Temperature 33
2.5 Temperature Dependent Fluorescence Evaluation of Europium 36
2.6 Temperature Dependent Fluorescence of Terbium 39
2.7 Evaluation of the LIFT fluorescence chemicals 46
2.8 Evaluation of the Spectral Characteristics of Rhodamine B and 110 47
2.9 LIFT Ratiometric Methods for the Determination of Temperature 49
2.10 Temperature Dependence of Rhodamine B, Rhodamine 110 Solution 51
2.11 Fabrication of 488nm Light Source for Calibration of Rhodamine B-110 Solution 54
2.12 Effect of Concentration of Rhodamine B-110 Solution on Spectral Emission 56

Chapter 3: Application of LIFT and FERIT to Measure Temperature Fields On and Around Radiofrequency Heating Devices 59
3.1 Application of LIFT to Measure Temperature Fields Surrounding RF Probes 59
3.2 Image Acquisition Rate Improvement 63
3.3 Field Temperature Measurements Around RF Probes 66
3.4 Results of LIFT measurement in gel medium 70
3.4.1 Monopolar 70

3.4.2 Bipolar 71
3.4.3 Effect of Bubble Formation on LIFT Measurements 80
3.5 FERIT Measurements on the Monopolar RF Probe 82

Chapter 4: Conclusions and Future Work 86
4.1 Future Developments for Application of LIFT and FERIT to RF Heating ... 89
4.2 Future Application for the Low Temperature FERIT Method 90

Appendix A: Procedure for Terbium and Europium Preparation 94

Appendix B: Light Source Evaluation with Ocean Optics Spectrometer 97

Appendix C: Matlab Code for FERIT and LIFT Whole Field Analysis and AVI Creation 100

BIBLIOGRAPHY 102

LIST OF TABLES

Table 4.1: Comparison of conventional temperature measurement methods with fluorescent temperature measurements.....88

LIST OF FIGURES

Figure 1.1: Schematic of Bipolar and Monopolar Radiofrequency Heating 4

Figure 1.2: Thermocouple Response in a Radiofrequency Field 6

Figure 1.3: Experimental Configuration to Test the Presence of Water on IR Measurements 9

Figure 1.4: Effect of a Thin Fluid Layer on IR Thermometry 10

Figure 1.5: Diagram of a dorsal skin flap chamber mounted on a rat, an actual skin flap chamber, and measured isotherms by an IR camera resulting from low temperature treatment of the tissue in the window chamber. 11

Figure 1.6: Fluorescence and Phosphorescence Diagram (Jablonski Diagram)..... 13

Figure 1.7: Relationship Between Fluorescence Intensity and Quencher Concentration at Various Temperatures 18

Figure 1.8: LIFT Experimental Schematic 19

Figure 1.9: FERIT Experimental Schematic 21

Figure 2.1: Ocean Optics spectrometer sample holder with emission and excitation fibers mounted 90° with respect to each other. 25

Figure 2.2: Light Source Evaluation with Spectrometer 27

Figure 2.3: Radiofrequency probe coated with Europium (A), and plastic valve pintle coated with Terbium (B) and excited with a 365nm UV light source..... 29

Figure 2.4: Terbium Emission Spectra for Excitation at 254nm and 365nm 30

Figure 2.5: Fluorescent Emission Response of Europium and Terbium 31

Figure 2.6: Temperature Assignment for Measured Intensity Ratio 34

Figure 2.7: Comparison of Calibration Methods for the Europium Fluorophore 35

Figure 2.8: Europium Temperature Dependent Fluorescence Intensity Profiles Evaluated with a Digital Camera and Spectrometer 37

Figure 2.9: Comparison of FERIT Measured Temperature with Thermocouple Temperature 39

Figure 2.10: Temperature Dependent Fluorescence Intensity Profile of Terbium 41

Figure 2.11: Schematic of the temperature control system used to create a cryogenic flow environment. Not shown are the UV excitation source and digital camera.. 42

Figure 2.12: Comparison between thermocouple measurements and FERIT measurements from 24°C to –80°C. The linear line was added to emphasize the agreement between the data sets. 43

Figure 2.13: Condensation Detection with the Terbium Polymer Film 44

Figure 2.14: Ability of FERIT to Detect the Onset of Condensation at Low Temperatures 45

Figure 2.15: Rhodamine B and Rhodamine 110 mixed in saline solution without excitation illumination and with illumination by an Argon laser sheet (488nm)... 46

Figure 2.16: Emission response of Rhodamine B at Various Excitation Frequencies... 48

Figure 2.17: Emission Response of Rhodamine 110 at Various Excitation Wavelengths 49

Figure 2.18: Intensity variation of Rhodamine B, Rhodamine 110 solution 52

Figure 2.19: Fluorescence Ratio of Rhodamine B and Rhodamine 110 with Respect to Temperature 53

Figure 2.20: Evaluation of the Light Source Used for Calibration of Rhodamine B and Rhodamine 110 55

Figure 2.21: Spectral Emission Shift Due to Concentration of Rhodamine B 57

Figure 2.22: Intensity Ratio Dependence on Temperature with Varying Concentrations of Rhodamine B and 110 58

Figure 3.1: Schematic of Validation Test 60

Figure 3.2: Comparison of thermocouple measurements with LIFT temperature measurements. Inset picture is a gray scale LIFT image showing the location of the thermocouples and approximate location of the line profile. 62

Figure 3.3: Effect of Concentration of Rhodamine B and Rhodamine 110 on Emission Intensity 64

Figure 3.4: Image of monopolar and bipolar radiofrequency probes. Close up images show the details of the probe tips. 67

Figure 3.5: Image of monopolar RF Probe Submerged in an Optically Clear Gel Medium 68

Figure 3.6: Experimental Equipment for LIFT measurements indicating the laser beam path, RF probe submerged in an optically clear tissue phantom, RF generators, and digital camera. 69

Figure 3.7: LIFT Predicted Temperature Around the Monopolar RF Probe..... 70

Figure 3.8: LIFT Predicted Temperature Around the Bipolar RF Probe 72

Figure 3.9: Gel phantom experimental configuration with the laser sheet passing through the bottom of the glass test container. 73

Figure 3.10: Whole field temperature measurement in a gel and saline medium due to monopolar RF heating. Line indicates gel-saline interface. Image A is 1 to 2 seconds post activation and image B is 45 seconds post activation. 76

Figure 3.11: Measured power output for the RF monopolar probe in a gel-saline medium and in a saline solution only medium. 77

Figure 3.12: Whole field temperature measurement in a gel and saline medium due to bipolar RF heating. Line indicates gel-saline interface. Image A is 1 to 2 seconds post activation and image B is 100 seconds post activation. Arrows in image B indicate bubbles. 79

Figure 3.13: Bubble formation on RF monopolar probe tip. Bubbles create an optical disturbance that effects LIFT measurement. 80

Figure 3.14: Temperature measurement effect of bubble formation. The points around the probe tip represent the relative location of the measurements. 81

Figure 3.15: FERIT Measurements on the Surface the Monopolar Probe Tip..... 84

Figure 3.16: Comparison of FERIT Measurements with the Temperature Measured by the Thermocouple Embedded in the Monopolar Probe Tip 85

Figure 4.1: Potential application of low temperature FERIT to measure temperatures on the window chamber during cryosurgery in order to correlate temperature and thermal damage..... 91

Figure 4.2: GFP Tumor Qualitative Intensity Measurements During Freeze-Thaw Cycle 92

Figure 4.3: Temperature dependent fluorescence of GFP from –12°C to 60°C. 93

Figure B 1: Evaluation of the Spectral Emission of Electromagnetic Excitation Sources with the Ocean Optics Spectrometer.....98

Images in this thesis are presented in color

KEY TO SYMBOLS AND ABBREVIATIONS

c	Speed of light
D	Sum of the diffusion coefficients of fluorophore and quenchers
E	Energy
f_q	Quenching efficiency
F	Fluorescence intensity in the presence of a quencher
F_0	Fluorescence intensity in the absence of a quencher
h	Planck's constant
I	Intensity
k	Boltzman's constant
k_0	Diffusion controlled bimolecular rate
k_q	Bimolecular quenching constant
N	Avogadros number
Q	Concentration of the quencher
R	Molecular Radius
T	Temperature
x	x-coordinate
y	y-coordinate

Greek:

η	Solvent viscosity
λ	Wavelength
ν	Wavenumber
ν_f	Frequency
τ_0	Lifetime

Subscripts:

em	Emission
ex	Excitation
EXP	Experiment
REF	Reference

Abbreviations:

FERIT	Fluorescent Emission Ratiometric Imaging Thermography
GFP	Green Fluorescent Protein
IR	Infrared
LIFT	Laser Induced Fluorescence Thermography
RF	Radiofrequency
UV	Ultraviolet

Chapter 1: Introduction

Temperature measurement and acquisition is an indispensable requirement in many areas of research and industry ranging from engineering and science to medicine. There are many situations in these fields of study where an increasingly detailed knowledge of temperature has become a necessity for developing and improving the technologies of these industries. Some situations warrant the use of non-conventional temperature measurement methods since conventional methods, such as thermocouples, infrared cameras, and other commercially available temperature sensing equipment may provide too little detail about temperature fields. They also may be unable to provide data in harsh chemical or electromagnetic operating environments, and may be geometrically incompatible with the application. This has led to the development of new and innovative methods for measuring temperatures using luminescent chemicals. Luminescence is the general term that encompasses the processes of fluorescence and phosphorescence. The three terms are often used interchangeably. Fluorescence and phosphorescence are similar in that they both generally result in the emission of visible radiation commonly associated with black light posters and glow in the dark watch faces. For the remainder of this thesis the terms fluorescence and luminescence will be primarily used.

Fluorescent lighting and phosphor screens for televisions were some of the first uses for luminescent chemicals. Developers of these technologies sought luminescent

chemicals that would not lose their intensity as temperatures increased. As early as 1933, Neubert suggested the use of luminous paints as an indicator of temperature.[1] He noticed that the intensity of luminescence of certain chemicals diminished at high temperatures. This discovery has lead to the extensive study of the class of chemicals that luminesce, i.e. fluorescent material, in order to understand their temperature dependent characteristics. The common characteristic that allows these chemicals to be used as a temperature indicator is the generally inverse relationship between luminescent intensity and temperature.

This thesis describes the principles of fluorescence and the factors that affect fluorescent intensity. Methods for calibration and quantification of fluorescent intensity variation as an indicator of temperature are presented, and these methods are applied to measure temperatures on the surface and in the surrounding medium of radio-frequency heating devices. Additional methods for whole field surface measurements down to cryogenic temperatures are also explored. Two types of fluorescent thermography are explored: Laser induced fluorescence thermography (LIFT), and fluorescent emission ratiometric imaging thermography (FERIT). Both techniques use the fluorescent emission of specific chemicals as indicators of temperature. The LIFT technique is a volumetric method performed in a fluid or solid medium whereas the FERIT method is a surface temperature measurement method. The details of the techniques are described later in the thesis.

1.1 Introduction to Radiofrequency Heating

Over the last decade, sub-ablative thermotherapy applied by laser and radiofrequency heating has found ever-increasing application in orthopaedic and ophthalmologic surgery. The applications are: the treatment of the instabilities of the shoulder, ankle, knee and hip joints [2,3,4], elimination of discogenic pain in the spine [5,6], tissue welding [7], thermokeratoplasty [8,9], chondroplasty [10,11] and skin resurfacing [12,13].

Irrespective of the specific procedure applied, the aim of the therapy is the same: altering the configuration of the strain-damaged, pathological or congenitally anomalous soft tissue (whether it be skin, joint capsule, ligament, disc annulus, cartilage or cornea) in order to re-establish stability and function. The basic mechanism of this therapy is the heat-induced denaturation of the underlying collagenous network of the soft tissues. Heat-induced denaturation causes micro-structural transformation of the collagen molecule and produces a thermal stress field that is a function of the direction of the collagen fiber orientation. The thermal stress field formed changes the configuration of the tissue.

In the clinical setting, heat is applied by a laser or a radiofrequency (RF) probe swept on the surface of the target tissue. An irrigation solution is circulated around the target tissue in order to eliminate hot spots and to clean the debris. In laser heating, a Ho:YAG laser is usually preferred. In radiofrequency heating however, there are two alternatives. The first one is bipolar radiofrequency in which the active and the passive electrodes are located at the probe tip. The second choice is monopolar radiofrequency in which the active electrode is located at the tip of the probe and the return (patch) electrode is placed on the patient's skin. The two modes of radiofrequency heating are

illustrated in Figure 1.1. This figure shows a schematic of the monopolar and bipolar probes and shows the assumed general nature of the electrical field created between the positive and negative return electrodes.

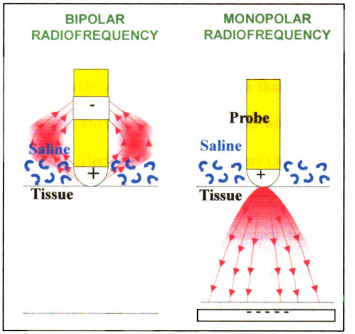

Figure 1.1: Schematic of Bipolar and Monopolar Radiofrequency Heating

Oratec Interventions supplied the monpolar radiofrequency unit and ArthroCare Inc. supplied the bipolar radiofrequency unit. During the operation, the surgeon sweeps the probe on the target until color change and shrinkage are observed. The success of the therapy is primarily based on the visual perception and the technique of the surgeon.

Collagenous tissue denaturation and shrinkage in response to heating by laser, microwave, radiofrequency devices and hydrothermy are extensively studied phenomena [14,15,16]. The amount and the extent of the irreversibility of tissue shrinkage (i.e., thermal-mechanical strain formation) depend on many factors. These factors include the thermal history (temperature and time) [17,18,19,20] as well as the mechanical

stress applied on the tissue during heating [21]. Other factors include the pH of the surrounding medium and electrolyte concentration [22] as well as the type of collagen [23], its hydration level [24], and the degree of cross-linking [25]. In other words, the amount and rate of heat deposition, coupled to the properties of the tissue and the surrounding medium govern the response at both the microscopic and macroscopic scales [26].

Creating accurate models and simulation tools that can predict the extent of thermal damage penetration into the tissue when treated with different clinical heating methods and examining the effects of clinical parameters (such as the amount of saline circulation, variations in probe sweep speed, power setting and control algorithms) on the outcome require extensive knowledge of the thermal fields generated by these probes. This requires measurement of the temperature profiles (and therefore calculation of the heat fluxes) created by these probes and temperature measurement of the probe tip surfaces.

1.2 Evaluation of Common Temperature Measurement Techniques

1.2.1 Thermocouples

Utilization of thermocouples in order to determine the temperature distribution on and around the probes was not feasible due to the RF field generated by these probes. Thermocouples are a convenient device for making accurate point measurements with fast acquisition rates and are well suited to measure temperatures at the cryogenic level up to 3000°C [27]. They are very easy to use and are an inexpensive means for temperature measurement. However, thermocouples lack the ability to make whole field measurements and potentially interfere with an experimental environment

such as a flow field or an *in vivo* surgical procedure. Thermocouples are also limited to the nature of the surrounding environment in which they operate. Corrosive chemicals and radiofrequency and microwave fields are known causes that result in faulty operation of thermocouples. Figure 1.2 shows the effect a RF field has on a thermocouple signal. A single uncalibrated thermocouple was placed within 5mm of the bipolar radiofrequency probe tip for a set point of "1". Temperature was acquired at 1 Hz with the RF generator off and while the RF generator was activated.

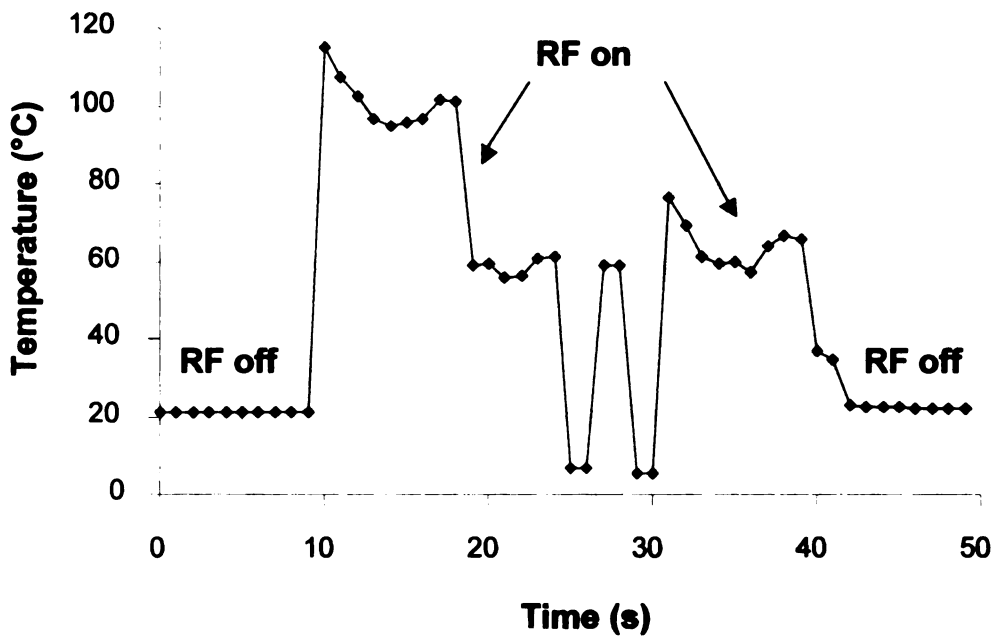

Figure 1.2: Thermocouple Response in a Radiofrequency Field

When the RF generator is turned on, the thermocouple signal becomes distorted and produces faulty data. The thermocouple signal is restored after the generator is turned off. The Oratec monopolar RF generator uses a T-type thermocouple embedded in the probe tip as a reference for its power control settings. The thermocouple signal is processed by a series of filters to reduce the noise produced by the radiofrequency

signal. The details of the filtering methods are unknown. It was observed in other experiments that the bipolar generator had a greater effect on thermocouple signal than the monopolar unit. This suggests it may be possible to filter thermocouple signals depending on the strength of the radiofrequency field, but there might still be some uncertainty in the temperature measurement depending upon the efficiency of the filter. Since one of the aims of this thesis is to measure whole field temperatures around radiofrequency heating devices, thermocouples were not deemed a viable means for temperature measurement.

1.2.2 Fluoroptic Thermometry

Fluoroptic thermometry was not feasible as well due to the relatively large size of the probes in the presence of large gradients. Fluoroptic thermometry is the optical analog to a thermocouple. It is similar to thermocouple measurements in that it measures temperature at a "point". Fluoroptic thermometry uses a temperature sensitive phosphor that has been applied to the end of a quartz optical fiber. Light pulses, which excite the phosphor, are launched down the optical fiber by a control unit and the resulting fluorescence decay response after each pulse is measured using the same optical fiber. The measured decay response varies according to the temperature of the tip of the optical fiber. Fluoroptic thermometry systems can measure temperatures from -200°C to 450°C and are capable of temperature measurements in harsh environments such as radiofrequency and electromagnetic fields.[28] However, fluoroptic thermometry is limited by its relatively slow sample rate of 4Hz and a relatively large fiber optic diameter of 1mm. The work described in this thesis uses similar fluorescent methods for whole field temperature measurement.

1.2.3 Infrared Thermography

Another alternative was using an Infrared (IR) camera. However, light at this wavelength is absorbed by the saline (both probes should be immersed in saline to operate) over very short distances and it was not possible to collect any information below the surface. IR thermometry equipment can provide whole field temperature measurement at framing rates up to or greater than 33Hz and is relatively simple to use since it is essentially a "point and shoot" method. They are often used in a preventative engineering fashion to monitor hotspots in applications ranging from industrial equipment to electrical circuit boards. IR can measure temperatures from -40°C up to 2000°C.[29] Due to the nature of thermal radiation; an electromagnetic wave traveling through a medium may become attenuated. If attenuation is such that no radiation emerges on the other side of the medium, the medium is known as opaque.[30] This property is also dependent on the thickness of the medium. Infrared radiation does not pass through media such as water and glass. This is unlike the visible spectrum, which readily passes through these media for considerable distances before any absorption takes place. This characteristic of infrared radiation makes it impossible to use an infrared camera to measure the temperature of an object submerged in water. The RF probes studied in this thesis are operated in saline solution at depths greater than 5mm from the surface. This depth is too great for infrared radiation to penetrate so the camera reports the surface temperature of the saline and cannot acquire temperature measurements around the RF probe.

A test was performed to determine the effect a thin layer of water covering a heated surface has on IR temperature measurements. The bipolar radiofrequency probe

was used to heat the underside of a bologna sample and temperature was measured on the opposite side with the IR camera and fluoroptic thermometer. This was initially done to gage the performance of the probes and to become familiar with their operation. The fluoroptic thermometer was in contact with the top surface of the bologna sample and the RF probe was in contact with the underside of the sample directly below the fluoroptic fiber as shown in Figure 1.3. The probe was activated and temperature measured by the IR camera near the fluoroptic fiber was compared to the measured temperature of the fluoroptic thermometer. A layer of water approximately 1mm thick was added to the surface and the same measurements were performed.

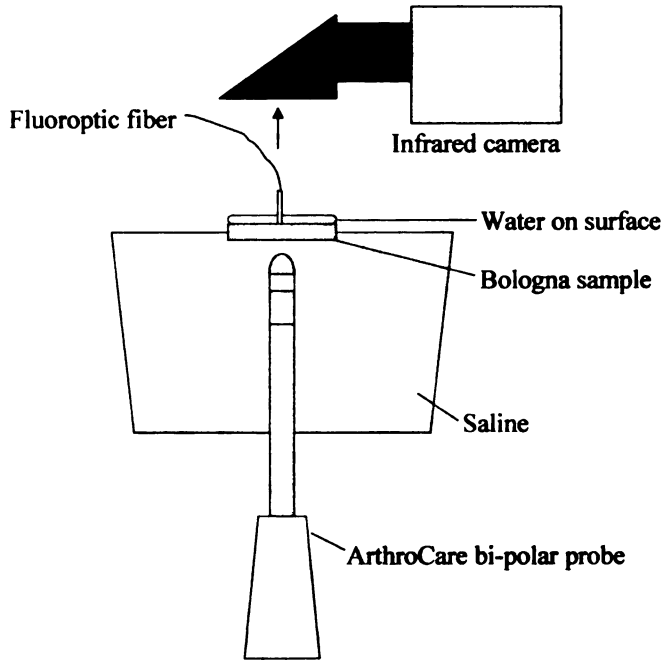

Figure 1.3: Experimental Configuration to Test the Presence of Water on IR Measurements

Figure 1.4 illustrates the effect the layer of water had on temperature measurement with an infrared camera when compared to measurements from a fluoroptic thermometer. The probe was activated for approximately 11s for both the wet and dry situations. The

results indicated water had the effect of damping the maximum temperature measured by the camera. For the dry situation, the IR camera and the fluoroptic thermometer agreed within 1°C of each other for the transient temperature cycle. When a thin layer of water was added to the surface the fluoroptic and IR camera differed by more than 10°C at the time of the maximum observed temperatures.

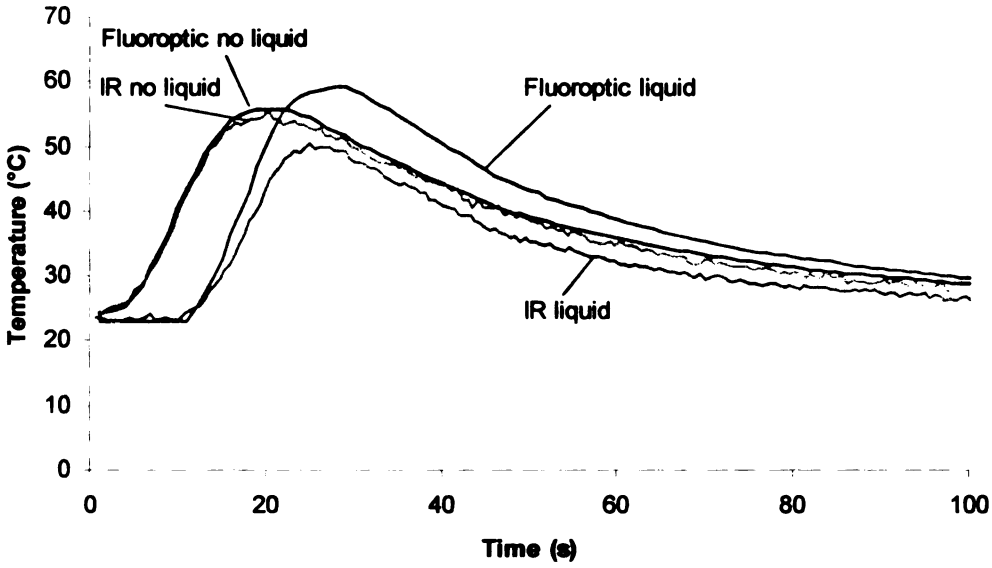

Figure 1.4: Effect of a Thin Fluid Layer on IR Thermometry

This makes it impossible to measure transient temperatures on a surface submerged in a fluid due to the thermal damping effects of the water and the opaque nature of water for relatively thin layers of water.

Therefore, in this thesis, an attempt has been made to utilize LIFT and FERIT as a method for measuring temperature fields in the surrounding medium and on the surface of monopolar and bipolar radiofrequency probes.

1.3 Introduction to Temperature Measurement at Cryogenic Levels

Whole field temperature measurement at cryogenic levels (-80°C) is desired since commercially available methods to make whole field measurements down to –80°C does not exist. Infrared cameras are limited to a minimum temperature of –20°C to –40°C depending upon the sensitivity of the IR detector. Thermocouples are capable of measurement down to cryogenic levels but can only provide point measurements and introduce fin effects especially for large thermal differences between the thermocouple tip and the ambient environment. Low temperature whole field measurements have utility in applications such as cryomicroscopy and the characterization of cryosurgical probes in tissue phantoms during freeze-thaw cycles. Figure 1.5 illustrates an example where whole field temperature measurement would be beneficial. Figure 1.5A is a diagram of a rat fitted with a dorsal skin flap chamber. The chamber as shown in Figure 1.5B is approximately 1 cm in diameter and is used for studying low temperature thermal treatments of tumors.

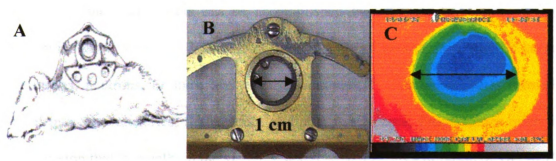

Figure 1.5: Diagram of a dorsal skin flap chamber mounted on a rat, an actual skin flap chamber, and measured isotherms by an IR camera resulting from low temperature treatment of the tissue in the window chamber.

Cryosurgery is performed on the tissue in the chamber and detailed temperature information is necessary for complete understanding of the resulting tissue damage. Figure 1.5C is a picture of isotherms in the window chamber resulting from treatment by a cryoprobe measured by an infrared camera. The minimum temperatures recorded were near -20°C, but lower temperatures were evident since the IR detector became saturated for regions out of its measurement range. However, new methods are needed to make the same type of measurements down to -80°C. Therefore fluorescent temperature measurement techniques have been developed to make it possible to perform whole field measurements at cryogenic temperature levels.

1.4 Fundamentals of Luminescence

Luminescence is the term that encompasses fluorescence and phosphorescence and they are often used interchangeably even though there are specific differences. Luminescence is generally described as the emission of light from any substance that occurs from electronically excited states. [31] A substance is caused to luminesce by an influx of energy to the substance, which causes the electrons to become excited to a higher electronic state. This can be accomplished by exposure to electromagnetic radiation including visible and ultraviolet light, x rays and gamma rays, particle beams of electrons, neutrons, or ions, and electrical currents.[32] Luminescence is formally divided into two categories, fluorescence and phosphorescence. Fluorescence refers to light emission that is usually in the visible spectral band and has a duration of 10^{-9} to 10^{-3} s, whereas phosphorescence is associated with a longer duration, typically $10^{-3} - 10^{3}$ s. A common test to determine if a material is fluorescent or phosphorescent is to simply

excite the material with the excitation source. If the material continues to luminesce after the excitation source is turned off, the material is phosphorescent. The material is fluorescent if the luminescence decays rapidly or immediately after the excitation source is turned off. Figure 1.6 is an energy level diagram or Jablonski diagram and is a physical representation of fluorescence and phosphorescence. Before excitation, the electrons in a material are populated in the ground state. In order for excitation to occur, a means to deposit energy (a photon) is needed and is most often in some other form of electromagnetic radiation such as visible or ultraviolet light. When a photon is absorbed, the electrons transition from the ground state to an excited state of the same spin multiplicity (S1 or S2).[33]

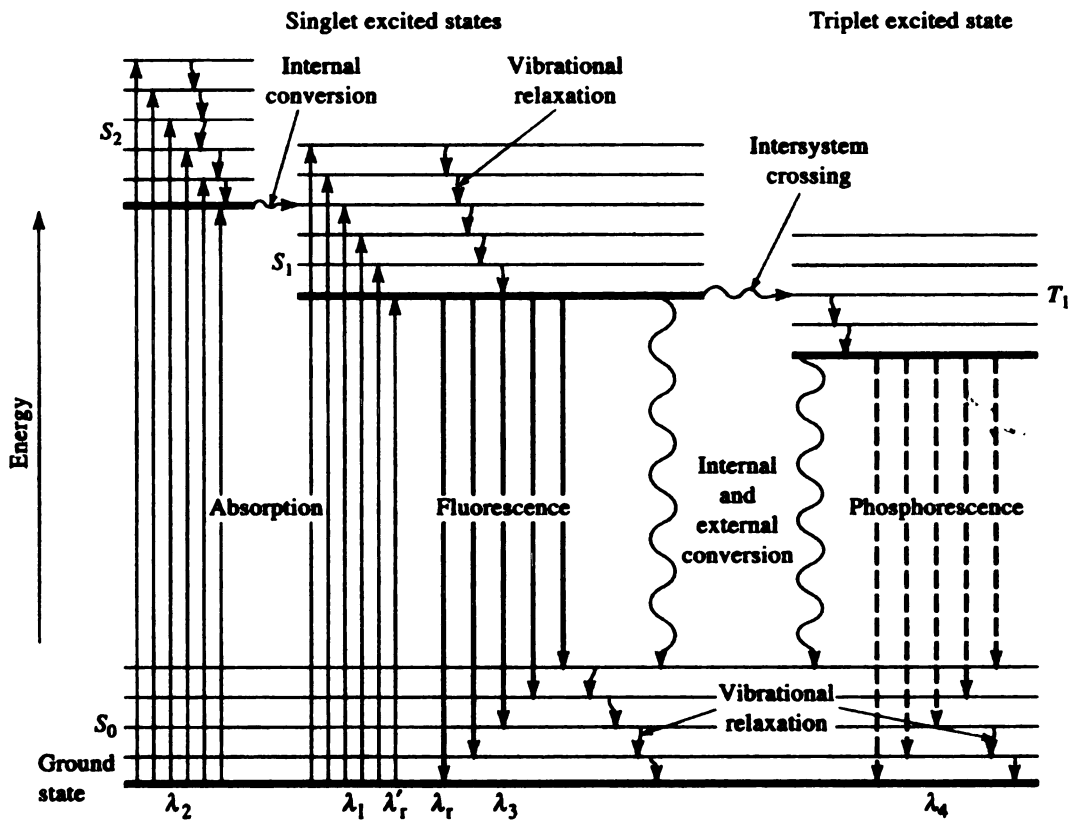

Figure 1.6: Fluorescence and Phosphorescence Diagram (Jablonski Diagram)

The excited electrons now undergo vibrational relaxation as a result of the vibrations in the molecule and collisions with surrounding molecules and solvent. The electrons relax to the ground vibrational level in their respective energy level they are located in with out any fluorescent emission. This takes approximately 10^{-12}s. Internal conversion follows next where the electrons transition between electronic states (S2 to S1). This is dependent on whether the electron was initially excited to the S1 or S2 state. From the ground vibrational level of the S1 excitation state, the electron can return to the ground state (S0) by emitting a photon. This is known as fluorescent emission and can only occur due to transitions from the S1 state to the S0 state. The excited electrons in the S1 state can also undergo spin conversion resulting in the formation of a triplet state, T1. This is described as intersystem crossing. Transitions from the T1 to the S0 state are forbidden due to the mismatch in electron spin. This is why this transition takes much longer than a transition from S1 to S0. This phenomenon is known as phosphorescence and is the emission of light from a triplet-excited state. Emission rates are slow for this phenomenon and can take as long as several minutes as the excited phosphors return to the ground state. Whether radiative emission occurs from the S1 state or the T1 state the electrons undergo external conversion, which involves energy transfer or collisions between the excited fluorophore and the surrounding solvent or matrix. This serves to reduce the radiated intensity of the emitted photon. The Jablonski diagram in Figure 1.6 shows that the energy of emission is typically less than that of absorption so fluorescence and phosphorescence occur at lower energy levels or longer wavelengths than absorption wavelengths. This phenomenon is known as Stokes

shift since it was first observed by Sir G. G. Stokes in 1852. This phenomenon is also represented by the Einstein photoelectric law

$$E = h\nu_f = hc\nu = \frac{hc}{\lambda} \tag{1.1}$$

where E is the energy, h is Planck's constant, ν_f is the frequency, c is the speed of light, ν is the wavenumber, and λ is the wavelength[34]. Since h and c are constant, E and λ are inversely related to each other. A reduction in energy results in an increase in wavelength. The energy absorbed by an electron is not equal to that released by the electron since some energy is lost due to vibrations and collisions mentioned previously.

Fluorescence and phosphorescence emission have been found to be dependent upon certain environmental variables such as pH, pressure, temperature, oxygen concentration, etc.[31,32,35,36] These variables can be related to events such as the intensity of the radiated emission, the lifetime of the emission, and the spectral shift of the emission. The most common and convenient emission parameter used to measure variables such as the pH, pressure, and temperature is the intensity of emission. The work presented in this thesis focuses on the use of fluorescent chemicals to measure whole field temperature distributions by associating measured fluorescent intensity changes to changes in temperature.

1.5 Theory of Temperature Dependent Fluorescence

Several factors result in the decay or degradation of fluorescence intensity. These factors are known formally as quenchers of fluorescence. Quenching does not involve a permanent change in the fluorescent molecule rather it is a temporary degradation of fluorescence until the quencher diminishes. Quenchers can take the form of a physical material introduced into the environment or can be a phenomenological change such as a temperature or pH change. The addition of a foreign material to the environment of the fluorescent chemical increases the random collisional encounters between fluorophore and quencher. A temperature increase causes the fluorescent molecules to experience increased collisions with the solvent or matrix molecules. In either case, random collisional encounters between fluorophore and the quencher or environment are increased and this reduces the observable fluorescence emission. This unique characteristic of fluorescent chemicals enables them to be used to detect trace amounts of foreign material in a fluid in addition to thermographic measurement applications. This thesis does not focus on the detecting foreign particles in a solution but rather on the phenomena of temperature dependent fluorescence. The effect of collisional quenching can be described by the Stern-Volmer equation,

$$\frac{F_0}{F} = 1 + k_q \tau_0 [Q] \tag{1.2}$$

In this equation, F_0 is the fluorescence intensity in the absence of the quencher, F is the fluorescence intensity in the presence of the quencher, k_q is the bimolecular quenching constant, τ_0 is the lifetime of the fluorophore in the absence of the quencher, and Q is

the concentration of the quencher[31]. The bimolecular quenching constant, k_q, is dependent upon temperature via the following three equations.

$$k_q = f_Q k_0 \tag{1.3}$$

In this equation, k_0 is the diffusion controlled bimolecular rate and f_Q is the quenching efficiency. The term, f_Q, is a constant value and reflects how effective a collisional encounter is at quenching a fluorophore. The term k_0 is a constant given by,

$$k_0 = \frac{4\pi RDN}{1000} \tag{1.4}$$

where R is the collision radius, D is the sum of the diffusion coefficients of the fluorophore and quencher, and N is Avogadro's number. The diffusion coefficient, D, is given by,

$$D = \frac{kT}{6\pi\eta R} \tag{1.5}$$

where k is the Boltzman constant, η is the solvent viscosity, R is the molecular radius and T is the temperature. Equation 1.5 indicates that the diffusion coefficient increases with increasing temperature, which results in an increase in k_0 in Equation 1.4, thus increasing the bimolecular quenching constant, k_q, in Equation 1.3. This causes the ratio F_0/F in Equation 1.2 to increase thus denoting a decrease in intensity with temperature increase. Figure 1.7 is a plot of F_0/F versus [Q] with a slope equal to $k_q\tau_0$ for arbitrary scenarios. This plot illustrates a linear relationship between the quencher concentrations to fluorescence intensity. If the quencher concentration [Q] remains

constant throughout an experiment and temperature is increased, then temperature is the only parameter causing a decrease or increase in the fluorescence intensity value F.

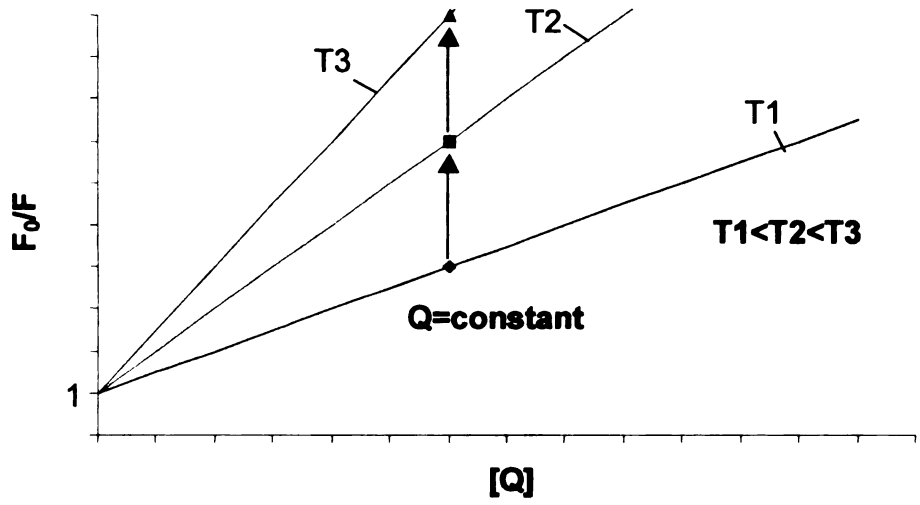

Figure 1.7: Relationship Between Fluorescence Intensity and Quencher Concentration at Various Temperatures

For the experiments in the following chapters the concentration of the quenchers remained constant therefore allowing direct correlations to be made between fluorescence and temperature for the LIFT and FERIT methods described next.

1.6 Introduction to LIFT

Laser induced fluorescence thermography is a temperature measurement method that uses a laser sheet to excite fluorescent chemicals in a solution or matrix. A laser is used since it can be converted into a sheet in order to excite a plane in the fluid medium. Incandescent light sources can also be used to excite the solution, but yield a volumetric average of fluorescent intensity and therefore a volumetric average of the temperature. An incandescent excitation source was used for calibration procedures presented later

when the fluid medium was maintained at isothermal temperatures. A sensitive detector, usually a high quantum efficiency digital camera or spectrometer, measures the fluorescent emission. The measured emission intensity is then converted to temperature based on calibration curves. Figure 1.8 is a schematic of the LIFT temperature measurement technique.

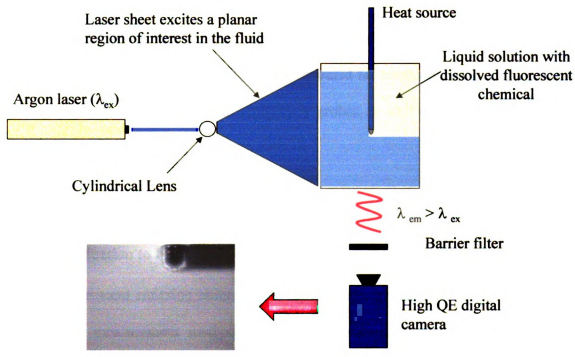

Figure 1.8: LIFT Experimental Schematic

A laser beam is transformed into a laser sheet with a cylindrical lens. The laser sheet 1mm thick excites a planar area in the fluid medium containing fluorescent chemicals that are excited by the wavelength emitted by the laser. For an incandescent light source, a barrier filter is used to separate the particular wavelength of light that excites the fluorescent chemicals in solution. The laser sheet can be positioned in any plane of interest but is illustrated as impinging the centerline of the submerged heat source so

that planar fluorescence intensity around the submerged heat source can be measured. The resulting fluorescent emission is separated from all other wavelengths of electromagnetic radiation with a barrier filter and the intensity of the emission is measured by a sensitive digital camera or spectrometer. The resulting fluorescence emission intensity is much less than that of the excitation source; so sensitive emission detectors are necessary. A digital camera produces a gray scale image as shown in Figure 1.8 and temperature is extracted at all points of illumination using calibration curve fit analysis. This method will be demonstrated for temperature measurement in a fluid medium surrounding the radiofrequency probes as well as within a clear tissue phantom.

1.7 Introduction to FERIT

Fluorescent emission ratiometric imaging thermography is a whole field surface temperature measurement method that uses fluorescent chemicals embedded in a polymer film coating as is illustrated in Figure 1.9. The fluorescent film can be coated on most non-permeable surfaces and is excited with an incandescent source with a barrier filter to select the desired excitation wavelength. The fluorescent emission intensity from the surface of the sample is measured with a sensitive detector with a barrier filter and converted to temperature in a similar manner as the LIFT method. The FERIT technique is suitable to measure temperatures for cryogenic applications as well as the high temperatures associated with radiofrequency heating.

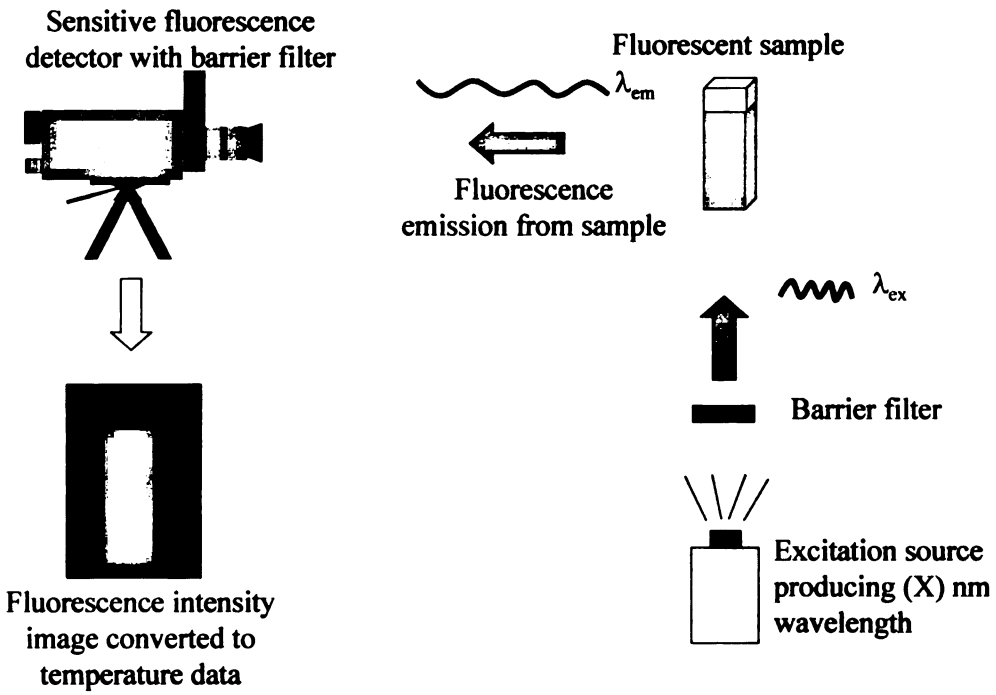

Figure 1.9: FERIT Experimental Schematic

This method will be demonstrated later on for surface temperature measurements on objects cooled to -80°C as well as for the radiofrequency probes heated to 85°C.

Chapter 2: Evaluation of Temperature Dependent Fluorescent Chemicals

The materials and procedures required for a fluorescent dependent temperature measurement system are relatively straightforward. The basic equipment needed is an electromagnetic energy source that causes the temperature dependent fluorescent chemical to be excited, a sensitive detector used to measure the resulting fluorescent emission and data acquisition equipment to record the detector output. Also needed is a means to calibrate the fluorescent intensity emission of the fluorophore with temperature. Many variables can affect temperature measurement with fluorescent chemicals so a complete understanding of the response of the fluorescent chemical is needed for the environment in which testing is to be performed. The first step in using fluorescent chemicals, as an indicator of temperature, is to select a chemical from the list of many known fluorescent chemicals, and to establish or verify that the chemical exhibits temperature dependent fluorescence within the temperature range of the specific application. There are many fluorescent chemicals that have been evaluated by other researchers so a literature search is an essential resource for chemical selection. The chemical must also be able to co-exist in the operating environment of the application. For example, some fluorescent chemicals are quenched by a pH change, so using a chemical in an environment with fluctuating pH and temperature may result in faulty measurements since pH and temperature would both affect fluorescence intensity

simultaneously. Based on previous research done in this lab and on a literature search, the fluorescent chemicals selected for evaluation of the FERIT method are Europium (III) Chloride, and Terbium (III) Chloride. See Appendix A for procedures regarding the chemical preparations of these compounds. Both Europium and Terbium exhibit strong temperature dependent fluorescence and are used individually for specific temperature ranges. Temperature is obtained with ratiometric methods described in detail in the next sections.

The chemicals selected for the LIFT method are Rhodamine B and Rhodamine 110. These chemicals are used in combination for a single temperature range. Rhodamine B exhibits strong temperature dependence and Rhodamine 110 is relatively temperature invariant. Rhodamine B and Rhodamine 110 fluoresce at different wavelengths and it will be shown later that the ratio between the respective fluorescence intensities produces temperature measurements that are presumably invariant with respect to experimental variables such as excitation source fluctuation and other optical aberrations. The Europium and Terbium are utilized in a polymer that is applied directly to a surface of interest by an airbrush, whereas the Rhodamines are utilized in a fluid as a volumetric indicator of temperature. The temperature measurement procedures for the liquid based and solid based fluorescent materials vary, so they will be divided into these sub categories for the proceeding discussions.

2.1 Evaluation of Fluorophores with a Spectrometer

A spectrometer is an instrument that measures electromagnetic radiation intensities for a range of wavelengths. Evaluation of the fluorophores with a spectrometer is essential in determining the optimum excitation wavelength of the fluorophores and for proper selection of barrier filters used for measurement of the emission intensities. The sensitivity of the spectrometer to particular wavelengths is dependent on specifications of the detector. The model used in this research, an S2000 spectrometer (Ocean Optics, Dunedin, FL) was capable of measuring wavelength intensities from low UV (250nm) to near IR (800nm). Wavelengths beyond these ranges were not encountered so spectrometer performance is unknown outside of this wavelength range. Some spectrometers are also capable of controlling the excitation wavelengths with 10nm or better bandpass control from UV to IR wavelengths. The Ocean Optics spectrometer came equipped with a dual excitation light source that allowed for UV and/or visible broadband excitation wavelengths. Specific excitation wavelengths could be achieved with barrier filters. Figure 2.1 shows an image of the spectrometer sample holder which is located at the center of the image and is sized to hold a $1cm^2$ cuvette for fluid analysis or solid fluorescent samples that are coated on a substrate of comparable size.

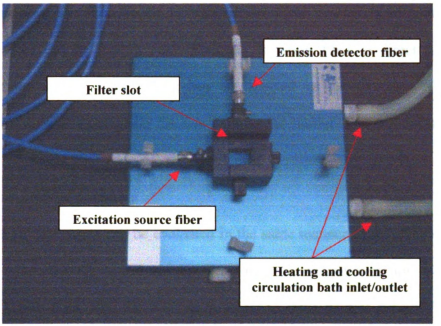

Figure 2.1: Ocean Optics spectrometer sample holder with emission and excitation fibers mounted 90° with respect to each other.

The sample holder is mounted onto a hollow aluminum base that allows the fluorescent samples to be temperature controlled by connecting a constant temperature circulation bath using the hoses at the right of the image. The circulation bath was capable of controlling the temperature of the specimens from −12°C to 100°C. The spectrometer sample holder can withstand temperatures from −100°C to +100°C. The manufacturer did not recommend temperatures outside of this range. A fiber optic cable directs light from an excitation source into the sample holder and the fiber optic 90° clockwise from the excitation fiber optic directs all emitted wavelengths from the fluorescent sample to the spectrometer detector for signal processing.

In addition to evaluating fluorescent specimens, the spectrometer is useful for evaluation of barrier filters and excitation light sources. A barrier filter can be placed in the slot denoted in Figure 2.1 in front of the emission detector with an excitation source

that encompasses the wavelengths of the barrier filter pointed directly at it. The excitation fiber can be moved 180° from the emission fiber to direct light at the emission fiber or any light source can be directed at the emission fiber. The spectrometer should only register the wavelengths the barrier filter transmits. Thus the manufacturer's specifications of the particular barrier filter can be verified or discredited.

Excitation sources can be evaluated in the same manner except the barrier filter should be replaced with neutral density filters to avoid saturation of the spectrometer detector. While evaluating the light sources, up to three neutral density filters with 2.5%, 4.0%, and 20% transmission were used at one time for an intense excitation source. This filtering resulted in spectrometer integration times on the order of 10ms. The dual excitation light source equipped with the spectrometer was evaluated with its own the detector to determine the specific wavelengths produced by the source in order to verify manufacturer specifications. This was done because during the process of evaluating some of the fluorescent samples, additional emission peaks were sometimes observed dependent upon the particular excitation source being used. Since the location and magnitude of the emission peaks are of critical importance in evaluating the temperature dependence of a fluorescent chemical, a thorough evaluation of the excitation sources was performed and the comprehensive results can be found in Appendix B. The light source supplied with the Ocean Optics spectrometer is equipped with Deuterium and Tungsten bulbs. The wavelength specification listed for the Deuterium bulb was 200 to 400nm and the Tungsten bulb was 360 to 850nm. Figure 2.2 shows the results of the light source evaluation with the Ocean Optics spectrometer.

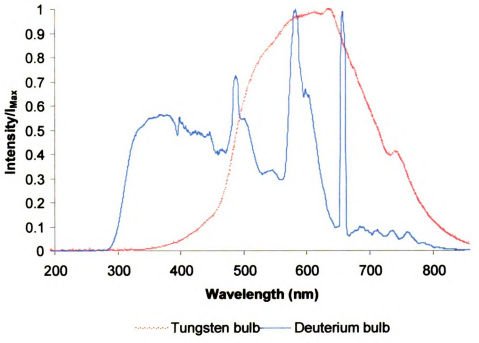

Figure 2.2: Light Source Evaluation with Spectrometer

Light sources were evaluated by lining up the detector fiber cable with the light source. Neutral density filters were placed in between the detector and light source as needed to prevent the detector from becoming saturated. Figure 2.2 indicates that the Deuterium bulb supplied with the spectrometer produced wavelengths that extend beyond the UV range. This particular source was initially being used to evaluate the Terbium and Europium compounds since those specimens are excited by ultraviolet radiation. It was assumed that the Deuterium excitation source produced wavelengths in the UV region only. During initial evaluation of Terbium and Europium with the spectrometer, emission peaks at wavelengths different from published spectra data were recorded by the spectrometer in the visible spectra region. These emission peaks were thought to be fluorescent emission from the sample, however they were a result of the excitation

source. This illustrates the importance of characterizing the excitation source so that the fluorescence experiments will not contain emission artifact.

2.2 Evaluation of the FERIT Fluorescent Chemicals

As indicated previously, the Europium and Terbium have been utilized in solid form as a surface coating or "fluorescent paint". The Europium and Terbium compounds are chemically prepared in the lab by procedures indicated in Appendix A and are dissolved in an organic solution containing dissolved PMMA pellets. While still in solution the compound is airbrushed onto the object being tested. The solution dries leaving behind a thin, polymer coating with the Europium or Terbium embedded in the polymer. The film is applied to the object until a white frosting becomes evident on the surface. The object is then gently heated to approximately 70°C for a couple of minutes to "cure" the film on the surface. The Europium compound has been previously developed in the lab by Lian[37] and exhibits temperature dependence from 20°C to 90°C. The temperature range of the Europium compound was limited by the temperature range of the polymer film. The polymer film melts at temperatures greater than 90°C. It has been suggested that Europium can be used to measure temperatures up to 900°C.[38] The method has been extended to cryogenic temperatures by using Terbium, which has been shown to exhibit temperature dependent fluorescence down to -170°C.[39] The research presented here will validate the temperature dependence of Terbium down to -80°C and apply the Europium compound for measurement on radiofrequency probe tips. Figure 2.3A shows a radiofrequency probe coated with the Europium polymer film and Figure 2.3B shows a plastic valve pintle coated with

Terbium. The specific use of the pintle will not be discussed in this thesis due to non-disclosure issues but is presented for validation purposes of the temperature measurement method only.

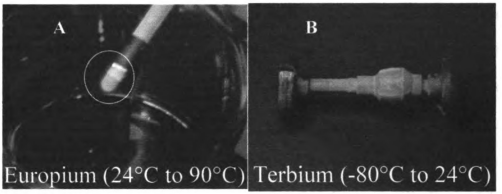

Figure 2.3: Radiofrequency probe coated with Europium (A), and plastic valve pintle coated with Terbium (B) and excited with a 365nm UV light source.

The samples are illuminated by the Opti Quip ultraviolet source with a 20nm bandpass filter centered at 365nm, and are imaged with a handheld Sony digital camera.

2.3 Spectral Evaluation of the Polymer Based Fluorophores with the Ocean Optics Spectrometer

Europium and Terbium are evaluated together since they are made in similar fashion, but they are different in their fluorescent response to temperature. Both fluorophores were evaluated with the Ocean Optics spectrometer by airbrush coating two pieces of aluminum 1.4cm x 1.4cm with the Terbium and Europium polymer compounds respectively. The coated sample was placed at a 45° angle in the sample holder. It has been suggested that the Terbium and Europium are excited by ultraviolet radiation.[32] Previous work with Europium performed in this lab by Lian[37] used the Opti

Quip UV source centered at 365nm and other cited research has suggested optimum UV excitation wavelengths ranging from 254nm to 378nm.[40] A study was performed to determine the effect the UV excitation wavelength has on the Europium and Terbium emission spectra. A new excitation source (Sirchie) that produced maximum intensity at 254nm, with smaller peaks located at 315nm, and 365 nm was tested against the original UV source that produced radiation at only 365nm with a 20nm bandwidth. This was done to determine if the emission output of Europium and Terbium could be improved by the higher energy excitation wavelengths included in the new source. The spectral output of the two light sources can be found in Appendix (B). Figure 2.4 is the resulting emission spectra of Terbium associated with excitation by the Sirchie (254nm) and Opti Quip (365nm) UV sources.

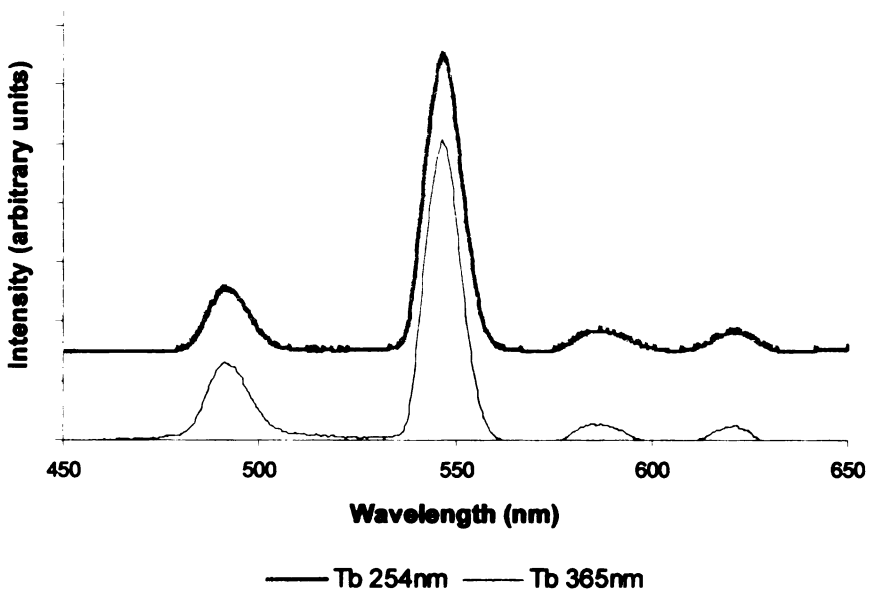

Figure 2.4: Terbium Emission Spectra for Excitation at 254nm and 365nm

The data sets have been normalized with respect to their own maximum intensities and have been shifted on the y-axis in order to distinguish between the two sets. The figure

shows that the emission spectrum of Terbium has the same emission peaks for either UV source, however the overall magnitude of emission intensity is dependent on the power of the particular excitation source and the integration time of the detector. The main emission peak of Terbium is located at 547nm or the green portion of the visible spectrum. Europium was evaluated next and Figure 2.5 shows the emission spectrum of Europium resulting from the excitation of the two UV sources. Europium has its main peak at 615nm, the red portion of the visible spectrum, with an additional emission peak at 595nm and further emission at wavelengths greater than 650nm. Optical bandpass filters were selected based on both emission plots so that fluorescence intensity from only the main emission peaks would be measured.

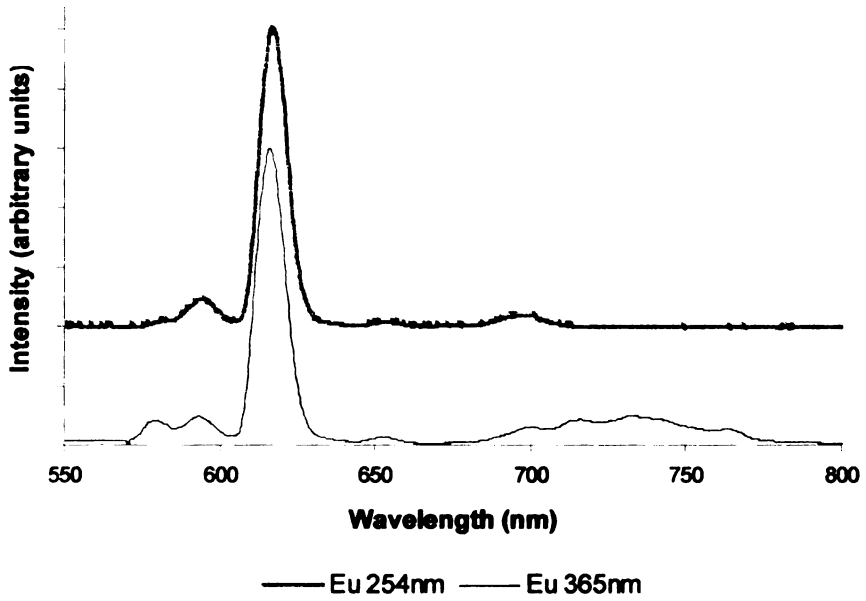

Figure 2.5: Fluorescent Emission Response of Europium and Terbium

A key point, in regards to the two UV light sources evaluated with the Terbium and Europium fluorophores, is that the 254nm source cannot excite a fluorescent sample

behind glass or submerged in water, whereas the 365nm source has the ability to excite the fluorophores through water greater than 10cm thick. Glass and water do not transmit the short UV wavelengths, therefore creating an obstacle for applications where the excitation radiation must pass through these materials. For this reason, the 365nm UV source will be used for the excitation of Terbium and Europium samples in future experiments.

The polymer-based fluorescent chemicals can be applied to most hard surfaces such as glass, metals, and plastics with an airbrush, which produces a thin, fluorescent film on the test specimen. The chemicals do not adhere well to porous and pliable surfaces such as biological material. The coated surfaces are relatively durable and are resistant to water and temperatures from –196°C to 90°C. The polymer films have been successfully submerged in liquid nitrogen, but they begin to melt at temperatures above 90°C. The fluorescent compounds of Terbium and Europium have been embedded in other materials, which have greater temperature resistant capabilities.[41] During the application of the fluorescent film, it is difficult or impossible to ensure even distribution or concentration of the fluorophore on the surface of the test object. This uneven distribution produces noticeable variations in fluorescence emission intensities for isothermal conditions. See Figure 2.3 for an image where the polymer film coating is uneven. The methods described in the next section show how non-uniform fluorophore concentration and other optical anomalies are eliminated by ratiometric methods.

2.4 FERIT Ratiometric Methods for the Determination of Temperature

The FERIT method measures fluorescent intensity and converts measured intensity changes into temperatures. The ratiometric approach to the thermography method ensures that the measured fluorescent intensity changes are due to temperature changes only and not other experimental variables such as excitation source fluctuation, non-uniform local concentration of the fluorophore, optical aberrations such as shadows or dust particles, and the solid angle involved when imaging a curved surface.

For an experiment occurring between T_{min} and T_{max} arbitrary temperatures, the following procedures are followed. The specimen is maintained at an isothermal starting point, usually room temperature, and verified with calibrated thermocouples. The sample is then illuminated with the excitation source and imaged with the digital camera or the intensity is measured with the spectrometer. The intensities in the image are denoted I_{max} if the Europium compound is used and is denoted I_{min} if the Terbium compound is used. This is because Europium has its maximum intensity at room temperature and Terbium has its maximum intensity at −80°C. The actual test then proceeds where the sample is cycled within the temperature range of the particular fluorophore being used and imaged at pre-determined time intervals dependent upon the transient nature of the experiment. After the test, an isothermal image at the other extreme of the temperature range needs to be taken. This requires isothermal control of the experimental system and is often the most difficult data point to implement in an experiment. For example, a sample coated with Europium would be held at a temperature higher than the temperatures in the experiment. The T_{max}, (I_{min}), endpoint usually ranges from 80°C to 90°C for Europium. Once the endpoint image is taken,

temperature can be extracted from all images by performing the following operation at each pixel:

$$\frac{I_{image(i,j)} - I_{\min(i,j)}}{I_{\max(i,j)} - I_{\min(i,j)}} = I_{ratio(i,j)} \qquad \textbf{(2.1)}$$

The intensity ratio is then compared to the intensities in the calibration data and assigned a temperature value as illustrated in Figure 2.6.

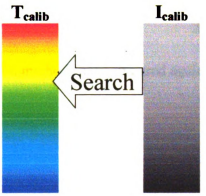

Figure 2.6: Temperature Assignment for Measured Intensity Ratio

This method measures the magnitude of the overall intensity change from T_{min} to T_{max} and assigns a temperature based on the percent change in intensity between the maximum and minimum intensities. For an arbitrary situation of two independent tests conducted over the same temperature range, it is possible to have one test experience an overall magnitude change of 100 and the other test yield an overall change of 1000. Corresponding temperatures for each test will have different absolute intensities but have the same intensity ratio per Equation 2.1.

Other ratiometric techniques were also performed with the FERIT method that made experiments easier to conduct. These involved only the initial isothermal

reference image to extract temperatures. The intensity for the initial isothermal condition is imaged and used as the only reference frame for the entire experiment. Equation 2.2 is used to create an intensity ratio. From this, a temperature is assigned from calibration data in the same fashion as the first ratiometric method.

$$\frac{I_{image(i,j)}}{I_{ref(i,j)}} = I_{ratio} \tag{2.2}$$

The two ratiometric calibration methods are compared against each other in Figure 2.7 for a sample size of n=4.

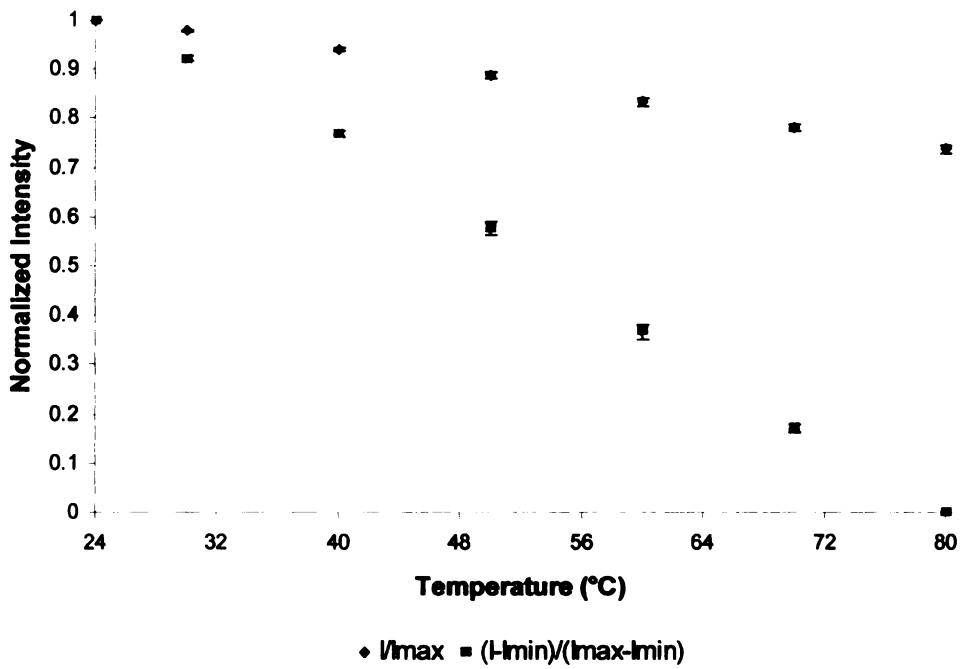

Figure 2.7: Comparison of Calibration Methods for the Europium Fluorophore

The two methods produce different curves but the data show that both methods are reproducible. The first ratiometric method (Equation 2.1) proved to be universal for any specimen being tested. This will be shown in Figure 2.8 where multiple samples were tested and shown to produce the same calibration curve. The second method (Equation 2.2) however does not exhibit reproducibility from sample to sample. This means that a specimen coated with the fluorophore must be calibrated prior to the actual test. The calibration is specific for the test specimen. On the positive side, a second reference intensity image at the opposite temperature extreme does not need to be taken with this method, thus eliminating the need for additional temperature controls.

2.5 Temperature Dependent Fluorescence Evaluation of Europium

The temperature dependent fluorescence of Europium was measured previously in this laboratory with the Spectra Source digital camera and barrier filter by Lian[37]. The same sample was evaluated three years later by similar methods to acquaint the author with the thermography technique and to evaluate the durability of the fluorescent film. The sample consisted of a 1mm thick, 5cm x 5cm, aluminum sheet that was coated with the Europium polymer compound attached to an electric foil heater of the same dimension.

An experimental configuration similar to Figure 1.9 was used. Using a heater, the temperature of the sample was increased in steps between room temperature, 24°C, and 80°C at approximately ten-degree increments. A calibrated foil thermocouple attached to the aluminum sample provided the independent reference temperature

measurement. Fluorescence intensity was measured in gray scale format by a sensitive digital camera when the sample reached equilibrium for each set point temperature. The Europium sample prepared for the spectral evaluation section of this chapter was also cycled from 24°C to 80°C with the temperature control of the spectrometer. A calibrated thermocouple was attached to the aluminum substrate and fluorescent emission was recorded at 10°C increments up to 80°C. Figure 2.8 compares the temperature dependent fluorescence intensity data obtained by the original researcher with the data obtained for the same specimen and experimental methods by the author. The data obtained for a new specimen using the spectrometer instead of the digital camera is also shown.

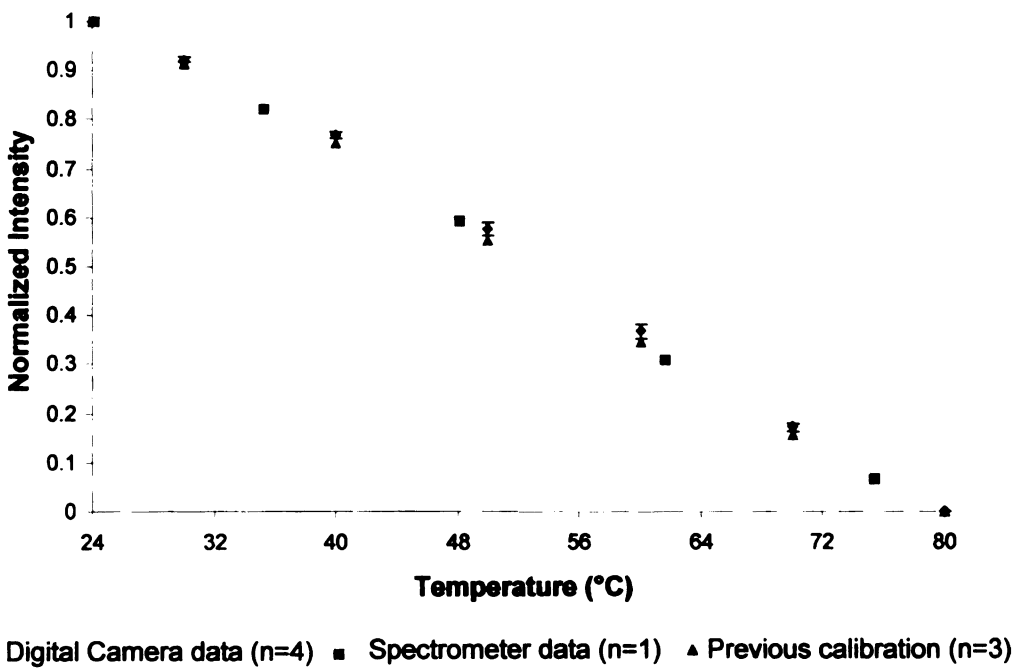

Figure 2.8: Europium Temperature Dependent Fluorescence Intensity Profiles Evaluated with a Digital Camera and Spectrometer

The three tests showed good agreement with each other even though two independent researchers used two evaluation methods over a three-year time period and used fluorescent chemicals from different processed batches. Figure 2.8 shows that the temperature dependent fluorescence characteristic of the Europium sample has a long shelf life of at least 3 years and that the calibration profiles are in good agreement independent of the experimental methods used to acquire the temperature dependent fluorescence emission intensities.

Another test was performed on a new test specimen in order to authenticate the validity of the calibration curves. The test specimen was a 3.5mm diameter cartridge heater that was coated with the Europium compound and instrumented with a foil thermocouple. The cartridge heater was cycled from 24°C to 80°C and gray scale intensity images were taken at steady state incrementally as the temperature was increased. The data were analyzed with the ratiometric methods described by Equation 2.1. A third order polynomial was fit to the calibration data with an R^2 value of 1 in Figure 2.8 and this was used to convert gray scale intensities measured on the cartridge heater into temperature values. The comparison between the temperatures predicted by the calibration curve fit (Figure 2.7) and those measured by the calibrated thermocouple are presented in Figure 2.9. A single pixel without signal averaging near the location of the thermocouple was used as the measurement point. A linear line was added to the plot to emphasize the agreement between the predicted and measured values. This experiment established confidence that the temperature dependent fluorescence behaved in the same manner for multiple fluorescent samples.

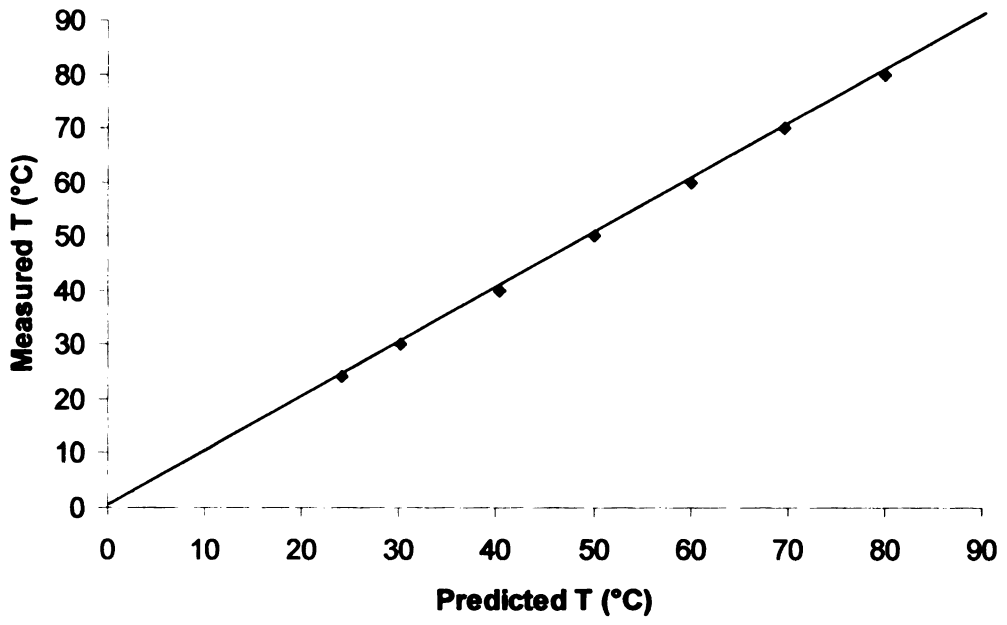

Figure 2.9: Comparison of FERIT Measured Temperature with Thermocouple Temperature

2.6 Temperature Dependent Fluorescence of Terbium

As mentioned earlier, a literature search suggested that Terbium has temperature dependent fluorescence intensity variation down to −170°C for Terbium dissolved in solvents not used in this research. The Terbium fluorophore was prepared in a similar fashion as the Europium compound and dissolved in an organic solvent (methyl ethyl ketone) with PMMA pellets. The details of the fluorophore preparation can be found in Appendix A. An aluminum substrate was coated with the Terbium-polymer film using an airbrush and evaluated at temperatures below zero to establish the temperature dependent fluorescence intensity correlation. For the particular application of interest, temperature measurement down to −80°C was desired. The coated aluminum substrate was mounted to a 5cm x 10cm hollow copper block through which dry Nitrogen gas,

cooled by a liquid nitrogen bath, was circulated. The flow of the cooled nitrogen gas was controlled using a flow valve. By adjusting the flow velocity of Nitrogen gas, the temperature of the test specimen could be lowered to temperatures below –100°C. Due to the low temperatures, the test environment needed to be purged of water vapor so that condensation did not create optical aberrations. Evacuation was accomplished by enclosing the fluorescent specimen, camera, and illumination source inside a plastic bag. The dry nitrogen exiting the cooling block was used to purge water vapor from the inside of the bag. Fluorescence intensity images were acquired at steady state temperatures in the same manner as the Europium experiments. A calibrated thermocouple was mounted to the aluminum substrate for reference and ratiometric methods, as described for the Europium compound, were used to establish a temperature versus fluorescence intensity emission curve. Isothermal conditions were observed when the thermocouple readout did not change in a 60s period during data acquisition. Figure 2.10 shows the temperature dependent intensity profile obtained with a digital camera for the Terbium sample (n=3). The temperature was lowered to –100°C but little intensity change was observed beyond -80°C.

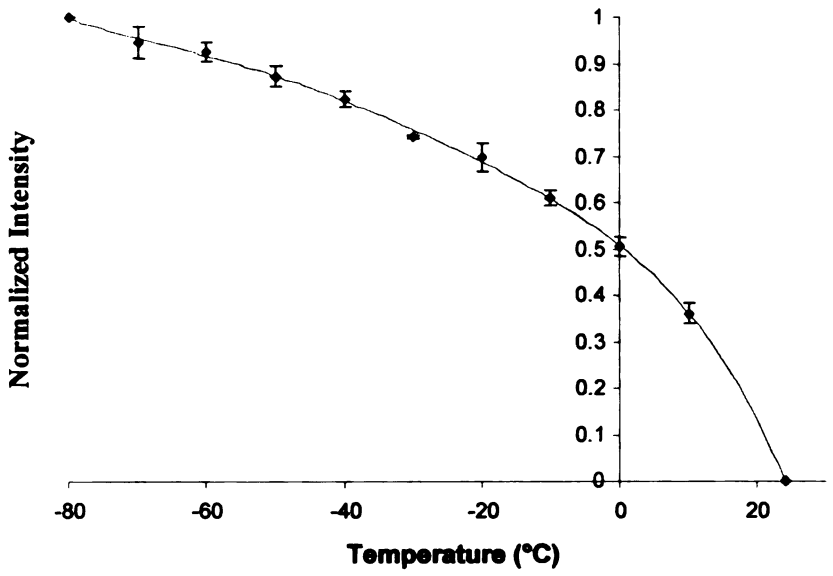

Figure 2.10: Temperature Dependent Fluorescence Intensity Profile of Terbium

A test was also conducted with the Terbium compound to evaluate the calibration data with a different sample coated with the Terbium polymer film. The plastic pintle shown in Figure 2.3 was used as the test specimen. The pintle is a part of an automobile pollution control valve through which air flows. The efficiency of the valve is subject to environmental conditions such as humidity and temperature. The goal of this work was to make "microscale" whole field temperature measurements down to cryogenic temperatures without obstructing the flow path. The material presented next represents a feasibility study performed evaluating the capability of using the FERIT method down to –80°C.

A temperature control system was developed so that the temperature of the pintle could be stabilized between room temperature and –80°C. The pintle was contained in a glass tube and temperature controlled dry nitrogen gas flowed into the

inlet and the exit flow emptied into the enclosed test area to facilitate vapor evacuation. A schematic of the details of the temperature control system is illustrated in Figure 2.11.

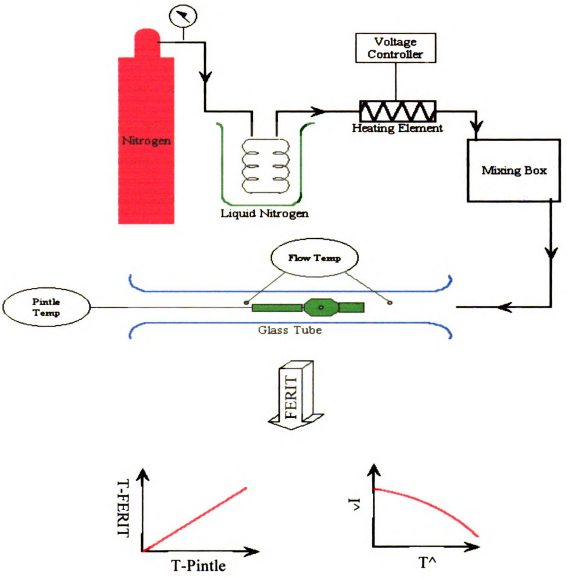

Figure 2.11: Schematic of the temperature control system used to create a cryogenic flow environment. Not shown are the UV excitation source and digital camera.

Nitrogen gas was first cooled to –196°C in a liquid nitrogen bath and then flowed through a portion of tube that contained a cartridge heater to warm the nitrogen gas to a

desired temperature. The gas then flowed through a handmade mixing box that promoted uniform temperatures upon entry into the glass tube containing the pintle. Temperatures in the tube were monitored by thermocouples upstream and downstream of the pintle. A third thermocouple was embedded in the center of the pintle. This thermocouple was used as the reference surface temperature measurement for the isothermal conditions when measurements were performed. Temperature was adjusted by controlling the flow rate of nitrogen gas and the voltage applied to the cartridge heater. A comparison between the embedded thermocouple measurements and the low temperature FERIT measurements are presented in Figure 2.12.

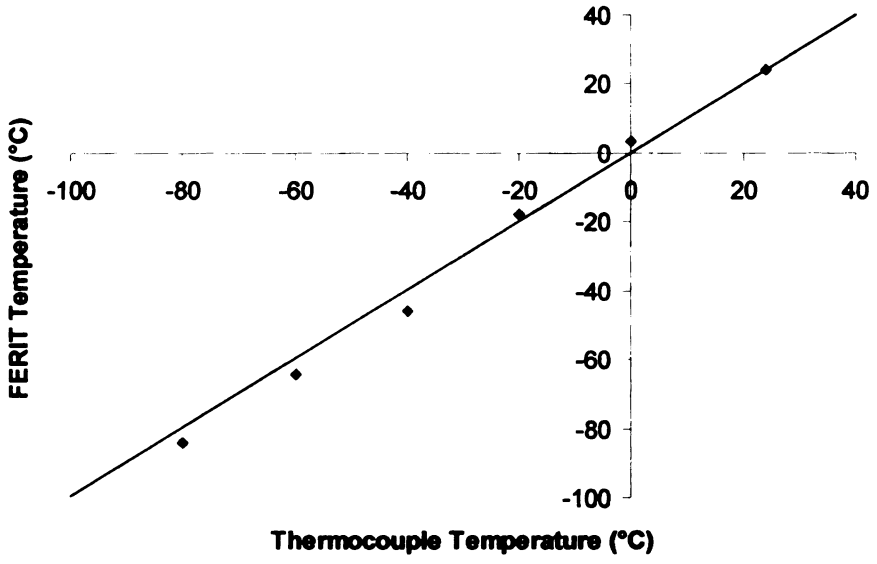

Figure 2.12: Comparison between thermocouple measurements and FERIT measurements from 24°C to –80°C. The linear line was added to emphasize the agreement between the data sets.

The measured FERIT temperatures are within 3°C of the thermocouple data. The difference in temperatures was attributed to the difficulty with maintaining an isothermal environment. The thermocouples located upstream and downstream of the pintle indicated temperature spikes related to instabilities in the flow of Nitrogen gas.

Handheld thermocouple readers used for the test had slow response rates, which probably produced a lag in the displayed temperature with respect to the actual temperature of the pintle. In addition to the slow response of thermocouple readers, the reference thermocouple was embedded within the pintle, creating another time lag for temperature measurement. Temperature control by conduction, as was done during the calibration tests, proved to be more stable than convection in validating the low temperature capabilities of FERIT.

Another part of this work was designed to assess the ability to detect the onset of condensation for a sample exposed to air with water vapor present. An aluminum sample coated with the Terbium polymer was mounted to a cooling block and cooled from room temperature to –40°C. Temperature measurements using FERIT and image processing software were made along a line defined across the coated sample. Figure 2.13 shows fluorescent intensity images at 7.7°C with no condensation and at –40°C with visible condensation formation.

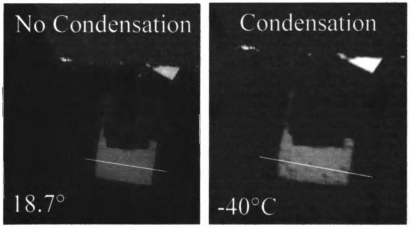

Figure 2.13: Condensation Detection with the Terbium Polymer Film

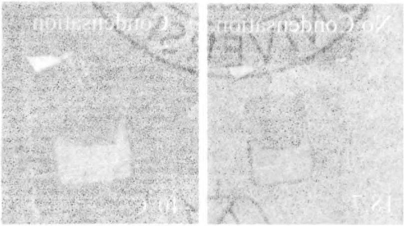

The temperatures measured by the FERIT method along the lines in the previous images are presented in Figure 2.14. The data show that, as temperature increases, the amount of apparent "noise" in the temperature measurements also increases. The quantification of the amount of noise in the fluorescence intensity images that would indicate the presence of condensation has not been performed. The data are presented as preliminary evidence that the current fluorescence measurement techniques may be useful with respect to quantitative detection of the onset and development of condensation and frost formation.

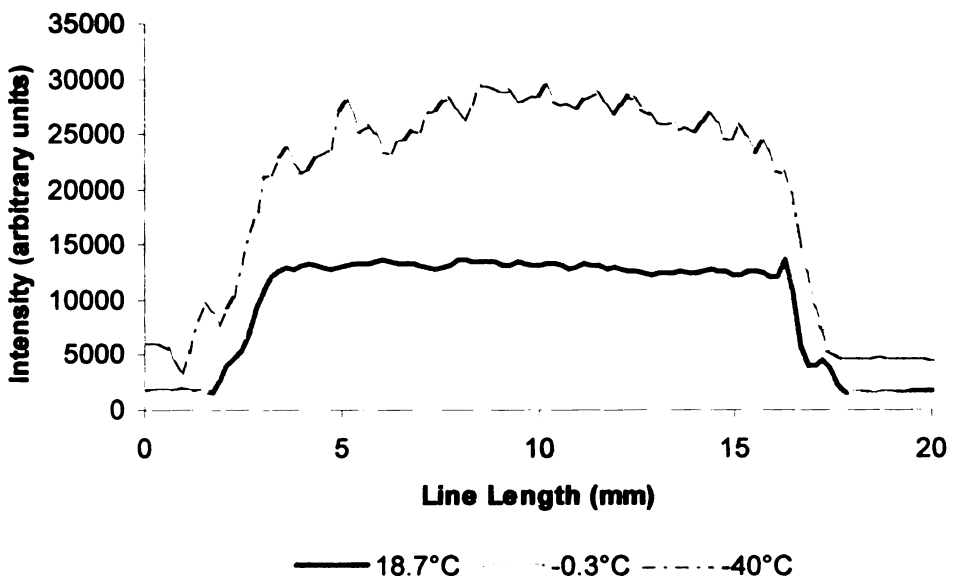

Figure 2.14: Ability of FERIT to Detect the Onset of Condensation at Low Temperatures

The material presented concerning the low temperature measurement capabilities of FERIT is not applied to any other application in this thesis. The technique has been developed and its feasibility has been established. The final chapter of this thesis describes future applications of the method.

2.7 Evaluation of the LIFT fluorescence chemicals

Rhodamine B and Rhodamine 110 are used in their manufactured form unlike Terbium and Europium, which must be manufactured by chemical processes in the lab. The Rhodamines are mixed in defined quantities in a solute and are used as a temperature indicator of the medium surrounding a heat source submerged in a liquid. Rhodamine B is the temperature dependent indicator whereas Rhodamine 110 is virtually temperature independent and acts as a reference to account for optical aberrations. These chemicals emit at two different wavelengths. By taking the ratio of the intensities of these two wavelengths, temperature can be quantified. The details of this approach are presented later in the chapter. Figure 2.15 shows a radiofrequency heating device submerged in saline solution mixed with Rhodamine B and Rhodamine 110 without illumination (A) and with the excitation source turned on (B). The excitation source for the Rhodamine compound is the 488nm emission line of an Argon Ion laser.

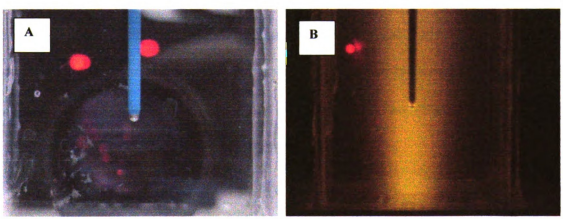

Figure 2.15: Rhodamine B and Rhodamine 110 mixed in saline solution without excitation illumination and with illumination by an Argon laser sheet (488nm)

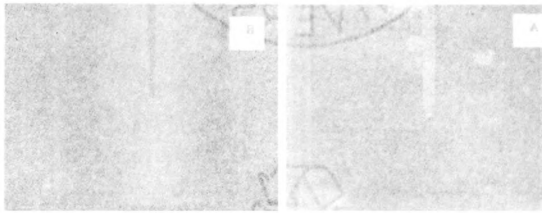
B
A

The concentration of the Rhodamines is such that the optical clarity of the solution is unaffected.

2.8 Evaluation of the Spectral Characteristics of Rhodamine B and 110

Evaluation of the spectral characteristics of the fluorescent materials in this thesis has been performed with a spectrometer. Two models of spectrometers were used for evaluation of the Rhodamine fluorophores. The first model is the F-4500 fluorescence spectrophotometer (Hitachi Instruments, San Jose, CA) and the second is the previously mentioned S2000 spectrometer (Ocean Optics). The F-4500 model was used for the initial evaluation of the Rhodamine chemicals to determine the excitation frequency that produces the maximum emission response from the compounds. The spectrometer has the capability to excite the test sample at all wavelengths of electromagnetic radiation from UV to near IR with 1 to 10nm bandpass widths. The excitation wavelength that produces the highest emission response can be determined in this fashion by scanning the excitation wavelength through a range of frequencies and measuring the resulting emission response of the chemical. Figure 2.16 shows the emission response of Rhodamine B with varying excitation frequencies. The left peaks are the excitation frequencies. The plot shows that the maximum emission intensity occurs using an excitation wavelength near 490nm.

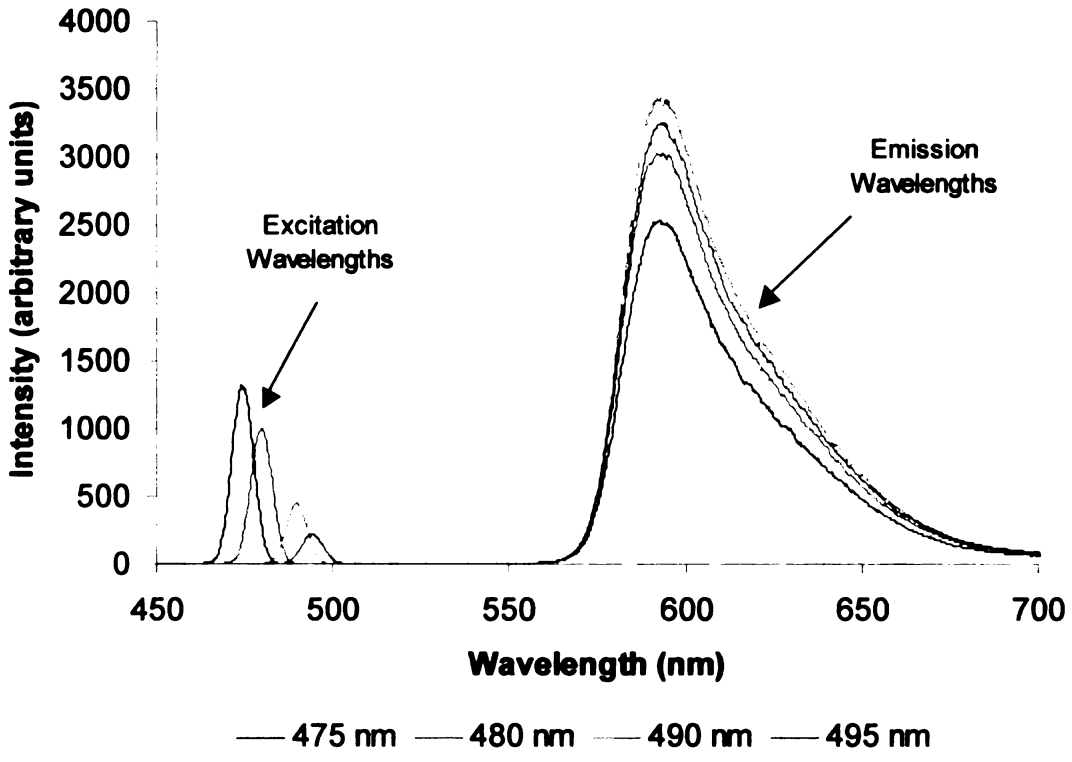

Figure 2.16: Emission response of Rhodamine B at Various Excitation Frequencies

The same experiment was conducted with a pure Rhodamine 110 solution. Figure 2.17 shows that Rhodamine 110 is excited by wavelengths from 475nm to 495nm with maximum emission occurring at 480nm excitation. Figure 2.16 and Figure 2.17 suggest that a common excitation wavelength between 475nm and 495nm can be used to excite both Rhodamine 110 and Rhodamine B. The most readily available coherent excitation source is the 488nm wavelength of an Argon Ion laser.

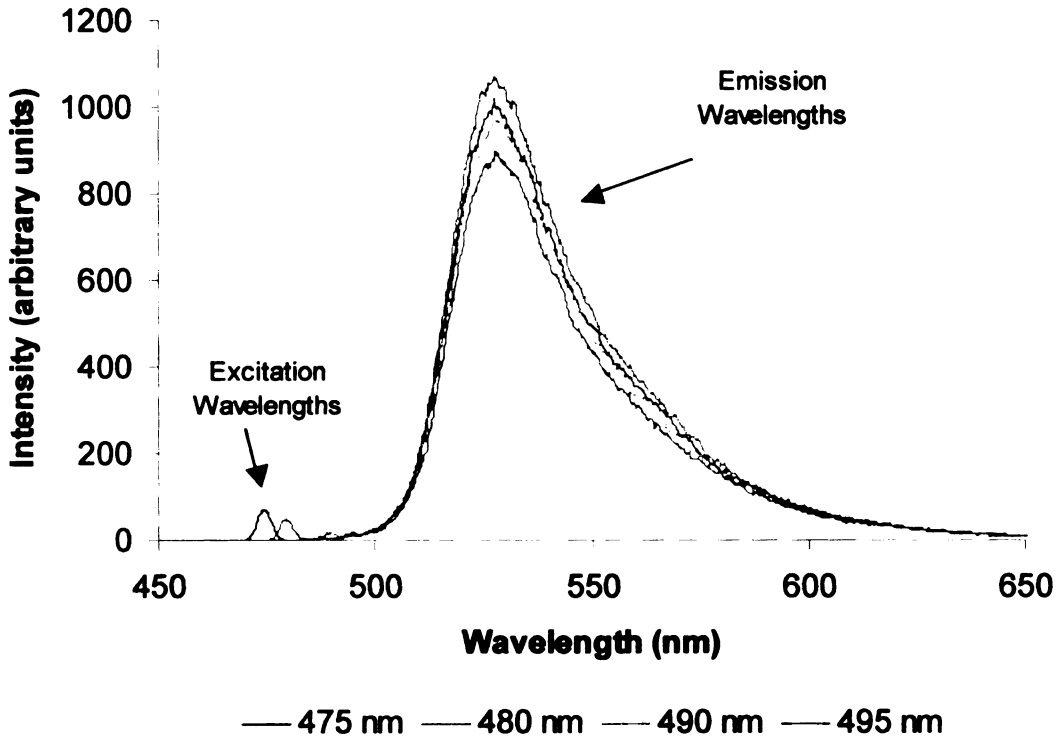

Figure 2.17: Emission Response of Rhodamine 110 at Various Excitation Wavelengths

2.9 LIFT Ratiometric Methods for the Determination of Temperature

The ratiometric techniques associated with the LIFT technique are similar to those presented for the second ratiometric method in the FERIT section. The LIFT method uses two fluorophores simultaneously in order to measure temperatures. The two chemicals used are Rhodamine B, a temperature sensitive fluorophores, and Rhodamine 110, a temperature insensitive fluorophores. The purpose of using two fluorophores is to reduce error resulting from intensity changes caused by parameters other than temperature. Since Rhodamine B and Rhodamine 110 fluoresce at different

wavelengths, any change in fluorescence intensity resulting from a non-temperature related parameter will be seen in both emission intensities of the fluorophores. The ratio of the emission intensities of Rhodamine B and Rhodamine 110 are taken as a measure of temperature so two images are taken for one temperature measurement. An automatic filter wheel under computer control was used to rotate a filter in place corresponding to the emission wavelengths of Rhodamine B and Rhodamine 110. Filters centered at 520nm and 580nm, 10nm bandpass, (Edmund Optics) were used in the filter wheel. The computer coordinated the position of the filters with the acquisition of the camera. At the start of an experiment, isothermal reference images are taken at room temperature and used as the divisor for all other intensity ratios. Equation 3 shows the operation performed to obtain temperature. The final I_{ratio} value is converted into temperature using calibration data.

$$\left(\frac{I_{RHB(i,j)}}{I_{RH110(i,j)}}\right)_{REF} \Rightarrow I_{REF(i,j)} \qquad \left(\frac{I_{RHB(i,j)}}{I_{RH110(i,j)}}\right)_{EXP} \Rightarrow I_{EXP(i,j)} \qquad \frac{I_{EXP(i,j)}}{I_{REF(i,j)}} \Rightarrow I_{ratio} \tag{2.3}$$

This method was suitable for steady state situations such as calibration procedures but proved to be too slow when transient data were desired due to the lag caused by using the filter wheel. For this reason, during transient acquisition only the Rhodamine B intensity emission was recorded and a ratio exactly like Equation 2.2 was used. This proved to be an effective means for fast temperature measurements. In order for the ratio of the two emission intensities to be recorded in an effective manner, two cameras are needed to operate simultaneously.

2.10 Temperature Dependence of Rhodamine B, Rhodamine 110 Solution

Evaluation of the temperature dependence of the Rhodamine B Rhodamine 110 solution was performed with the Ocean Optics Spectrometer. As stated earlier, the spectrometer sample holder was connected to a constant temperature circulation bath (Neslab). The bath can vary the temperature of the specimen in the sample holder from −12°C to 100°C. The manufacturer of the spectrometer does not recommend temperatures higher than 100°C. A solution of saline plus 0.05mgl^{-1} Rhodamine B and 0.0025mgl^{-1} Rhodamine 110 was placed in a quartz cuvette in the sample holder. The Rhodamine B-110 solution was known to have strong temperature dependent fluorescence from 15°C to 40°C.[42,43] The Ocean Optics spectrometer was used to establish the feasibility of using the Rhodamine B-110 solution to measure temperatures up to 90°C for the measurement of temperature fields surrounding radiofrequency heating devices. Previous results had only gone to 40°C. Starting from room temperature, the temperature of the Rhodamine solution was increased by ten-degree increments to 90°C. A thermocouple was mounted inside the quartz cuvette and a small magnetic stir bar and stirrer was used to create an isothermal solution. A 488nm light source was fabricated to excite the solution. The 488nm wavelength was chosen based on the initial emission response tests of the chemicals and the anticipation that a 488nm Argon laser will be used for the actual experiments. The next section describes the details of the fabricated light source for these experiments. Figure 2.18 shows the temperature dependent fluorescence of the Rhodamine B and Rhodamine 110 solution. The spectral output of Rhodamine B is located at approximately 580nm whereas the spectral output of Rhodamine 110 is located at approximately 520nm. Rhodamine B

exhibits fluorescence intensity decay as temperature is increased and Rhodamine 110 exhibits very little change with temperature variation. The intensity of Rhodamine B decreased by 70% from 20°C to 90°C and Rhodamine 110 decreased 3% from 20°C to 90°C. The Rhodamine 110 emission acts as an internal reference point to account for fluctuations in fluorescence not related to temperature.

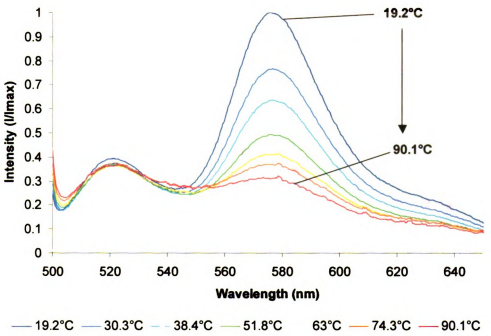

Figure 2.18: Intensity variation of Rhodamine B, Rhodamine 110 solution

If there is a change in the test environment such as a fluctuation in the excitation radiation source that affects the fluorescence emission of Rhodamine B then Rhodamine 110 should also experience a proportional change. By taking a ratio between the peak emission spectra of these chemicals, any variation in intensity of the light source or any other fluctuation should be removed.

The ratio of the intensity values of the Rhodamine B and 110 peaks are plotted against temperature in Figure 2.19. Regression analysis is applied to these data with Curve Fit 2D® or Microsoft Excel® in order to convert experimental ratiometric intensity data into temperature.

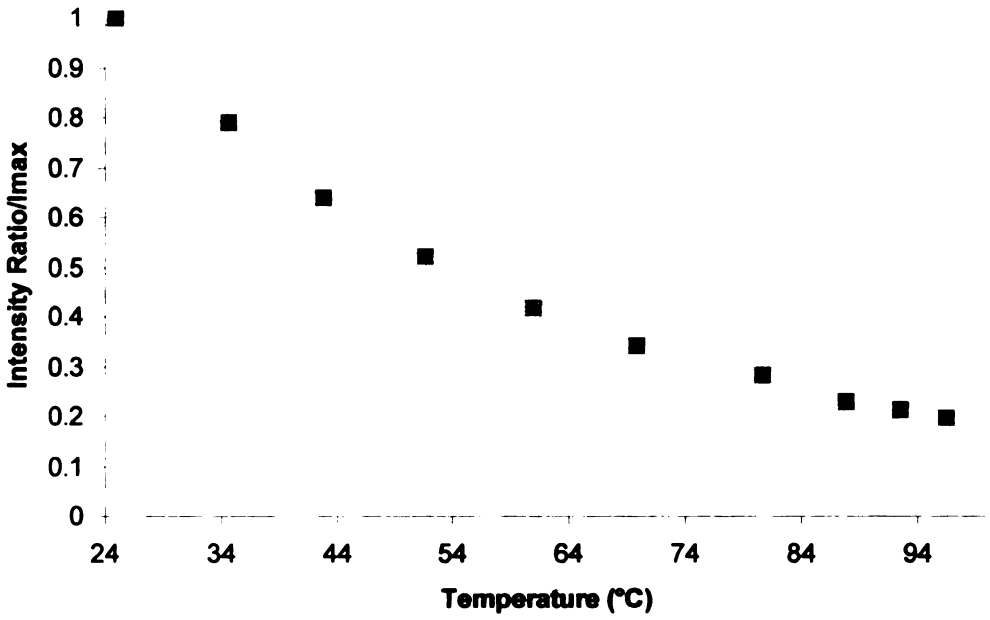

Figure 2.19: Fluorescence Ratio of Rhodamine B and Rhodamine 110 with Respect to Temperature

When the actual experiments are performed, a digital camera captures gray scale intensity images that are filtered to match the wavelengths of Rhodamine B and Rhodamine 110. Two images are actually taken, each filtered with a 10nm bandpass filter centered at 520nm and 580nm, to measure the intensities corresponding to Rhodamine B and Rhodamine 110. The ratio of the gray scale values is converted to temperature with a calibration similar to the one shown in Figure 2.19. Periodic

calibration was performed after a new mixture of Rhodamine B and Rhodamine 110 was made to ensure that the linear regression was still valid for a new fluorescent solution.

It should be noted that the locations of the peaks in Figure 2.18 are different from those of Figure 2.16 and Figure 2.17 for the excitation frequency evaluation of Rhodamine B and Rhodamine 110. The concentration of the Rhodamine B and 110 was much higher than what was used for the results in Figure 2.18. The exact concentration was unknown but a good measure to the extent of the concentration was the color of the solution. The color of the first test specimens was red for the Rhodamine B and yellow for the Rhodamine 110 whereas the solution used for calibration in Figure 2.18 was clear to a faint pink color. The fluorescent solution should contain the smallest amount of fluorescent chemical so that the chemical does not act as its own quencher. Basically, the darker the solution the harder it is for the emitted radiation to leave the solution in its original form. The fluorescent chemical in solution reabsorbs the emitted radiation and diminishes the radiated energy resulting in longer wavelengths exiting the test volume. A following section presents a discussion on the effect of concentration on temperature dependence.

2.11 Fabrication of 488nm Light Source for Calibration of Rhodamine B-110 Solution

A special light source was designed to excite the Rhodamine B and Rhodamine 110 solution since the light source supplied with the spectrometer was not powerful enough to produce a measurable emission response. This light source was used only

for the calibration experiments with the spectrometer. The light source consisted of a lamp house (Dolan-Jenner) with a bulb that emitted electromagnetic radiation from approximately 400nm to 750nm. A 488nm, 10nm bandpass, (Edmund Optics) filter was mounted in the light path to segment the desired wavelength of light. Figure 2.20 shows the spectral output of the light source without filtering and with the 488nm bandpass filter in place. The plots are normalized with respect to themselves. The intersection of the plots represents the portion of the unfiltered radiation that is being used as the excitation wavelength. This light source can be used for a wide range of excitation wavelengths using the appropriate optical barrier filters.

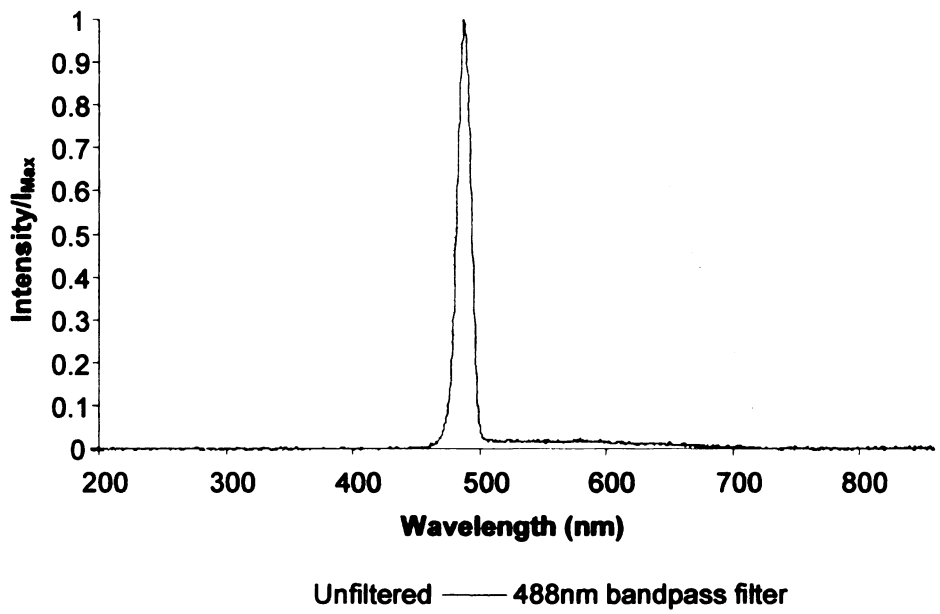

Figure 2.20: Evaluation of the Light Source Used for Calibration of Rhodamine B and Rhodamine 110

The light was conveyed to the fluorescent test specimen in the spectrometer sample holder with a 3mm diameter fiber optic cable instead of the 600μm diameter fiber optic

that was included with the spectrometer. The light collimator was removed from the excitation port of the sample holder so the larger fiber optic could be inserted into the holder. The emission port was left unchanged. This light source made it possible to analyze very low concentrations of Rhodamine B and 110 without using a high intensity source such as an Argon laser, which will be used in the application experiments.

2.12 Effect of Concentration of Rhodamine B-110 Solution on Spectral Emission

It is important to understand the effect the concentrations of Rhodamine B and 110 have on the temperature dependence. It has already been shown that a spectral shift exists for high concentrations of Rhodamine B in a solution from a comparison between Figure 2.16 and Figure 2.19. A fluorescent chemical absorbs the radiation from the excitation source and emits the energy at a longer wavelength than that of the excitation source. The emitted radiation is absorbed a second time by the excess fluorescent chemical in solution creating another spectral shift before final emission from the test volume.[31] Figure 2.21 plots the wavelength of the maximum intensity or peak of Rhodamine B measured by the spectrometer due to variations in the concentration. This plot shows an emission shift to higher wavelengths indicating an increased energy loss with increasing concentration of Rhodamine B. The spectral shift observed in Figure 2.21 also plays a critical role in optical filter selection. The spectrometer measures the intensity of all wavelengths but a digital camera must rely on filters to separate the individual wavelengths of light. If the maximum peak wavelength is shifted to a longer wavelength than the published wavelength then this is a good indication that the concentration of fluorescent chemical is too high. The temperature dependence of these

concentrations was also tested to understand the impact variations in concentration might have on a calibration curve.

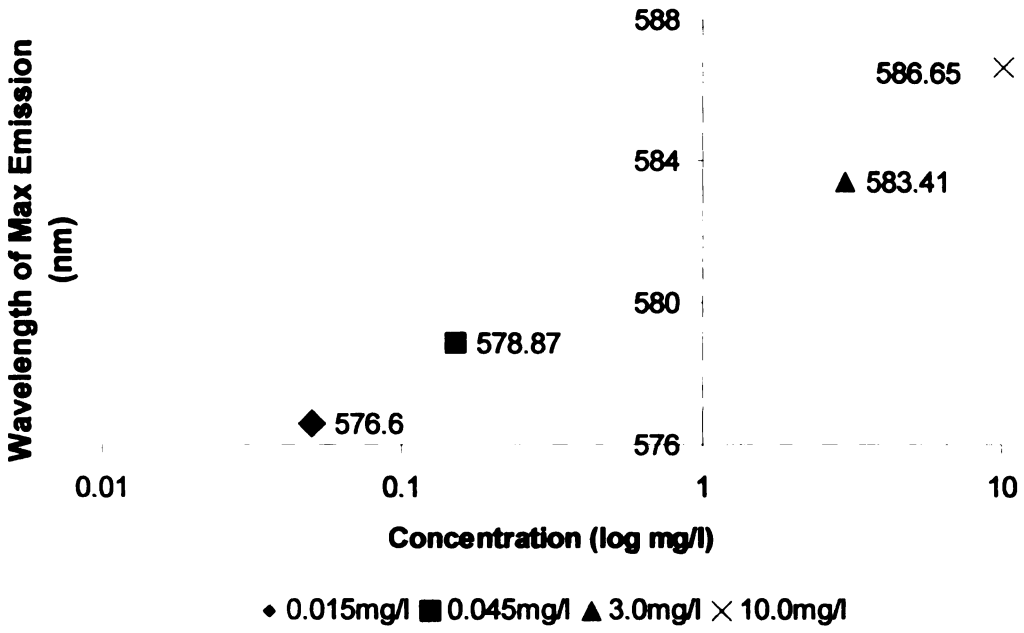

Figure 2.21: Spectral Emission Shift Due to Concentration of Rhodamine B

The lower concentrations are more susceptible to variation of the fluorescent chemical in the preparation of the solution since very small amounts of solute must be mixed with the solvent. Larger quantities of the fluorescent solution could have been made to reduce the frequency a new batch was made but other factors such as shelf life and potential contamination by other means may have been possible. The temperature dependence of Rhodamine B and 110 at varying concentrations is plotted in Figure 2.22.

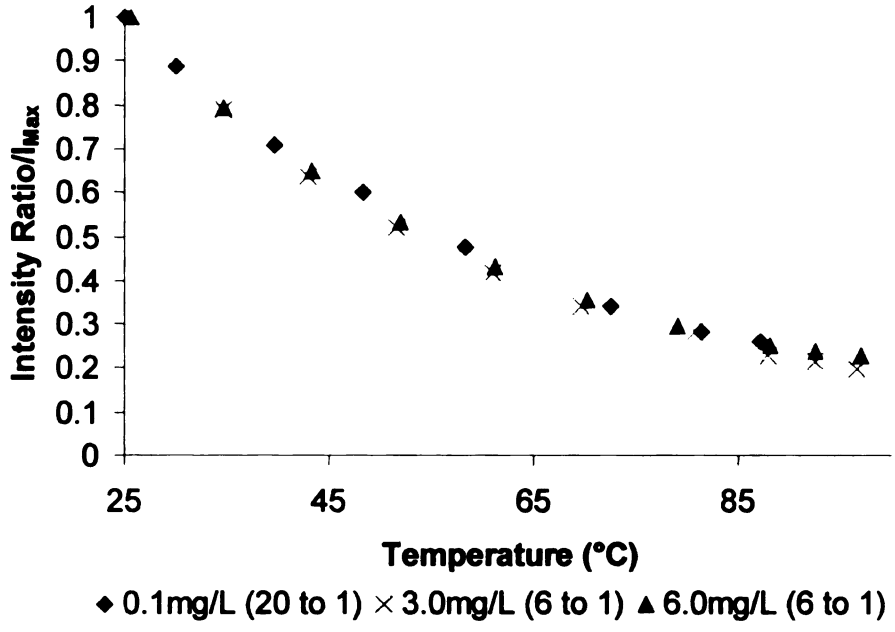

Figure 2.22: Intensity Ratio Dependence on Temperature with Varying Concentrations of Rhodamine B and 110

The concentrations are denoted in terms of Rhodamine B and its proportion with Rhodamine 110. All data were normalized with respect to the ratio of the intensity of Rhodamine B to 110 at 25°C. Figure 2.22 shows that the normalized temperature dependent intensity profiles are not affected by the concentration of the Rhodamine B and Rhodamine 110, thus simplifying the LIFT method greatly. This means that any quantity of Rhodamine B and Rhodamine 110 can be mixed in a fluid and temperature measurements can begin immediately.

Chapter 3: Application of LIFT and FERIT to Measure Temperature Fields On and Around Radiofrequency Heating Devices

3.1 Application of LIFT to Measure Temperature Fields Surrounding RF Probes

The measurement of the thermal fields surrounding radiofrequency heating probes is accomplished utilizing the temperature dependent fluorescence of Rhodamine B and Rhodamine 110 described in the previous chapter. Rhodamine B and Rhodamine 110 are excited by a large bandwidth of visible radiation wavelengths of light. In the previous chapter, the emission response for the two fluorophores was shown for several excitation wavelengths. This established a common excitation frequency between Rhodamine B and 110. The frequency of 488nm was selected since it produced high emission responses from both the fluorophores and it is a common wavelength produced by an Argon ion laser. The laser provides coherent, high-energy, narrow bandpass, electromagnetic radiation that enables large volumes of fluid embedded with fluorophores to be excited resulting in strong emission intensities measurable by sensitive cameras.

A validation test was performed with an immersion heater, a non-radiofrequency heating device, so that thermocouples could be used to verify the temperatures measured with the LIFT technique. This was done before temperature measurements on the actual radiofrequency probes were attempted to ensure that the LIFT technique

produced accurate results. Figure 3.1 illustrates the equipment used to validate LIFT. A cylindrical lens, 3.5mm diameter, was placed in the path of an argon ion laser beam, 0.5W, to produce a laser sheet approximately 1 mm thick. The laser sheet passed through the Rhodamine B and Rhodamine 110 solution and impinged on the centerline axis of the submerged immersion heater. A similar setup was also used for the radiofrequency probes.

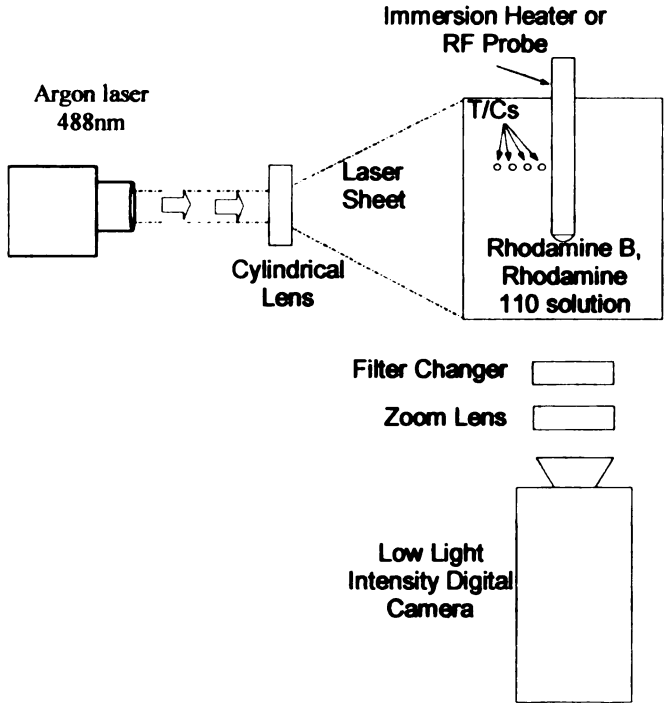

Figure 3.1: Schematic of Validation Test

Four thermocouples, 0.255mm diameter T-type, were positioned as shown approximately 4 mm from each other with the closest thermocouple being 0.5mm from the immersion heater. A low light digital camera (Cooke SensiCam) measured the emission intensity while a filter changer separated the emission spectra of Rhodamine B

and Rhodamine 110. From the previous chapter, Rhodamine B fluoresces at 576nm and Rhodamine 110 fluoresces at 520nm, so 580nm, 10nm bandpass and a 520nm, 10nm bandpass filters respectively were used in the filter changer. Reference images for both emission spectra were taken at room temperature before the immersion heater was turned on. After the immersion heater was powered, the thermocouples acquired time-temperature data at 1Hz and the digital camera acquired fluorescence intensity images at regular timed intervals, as the immersion heater produced temperature gradients in the saline medium. The images were later matched to the time-temperature data obtained by the thermocouples. During image acquisition, the filter changer automatically changed the filters in between shots so that the ratio of the Rhodamine B and Rhodamine 110 intensities could be performed after the test. Image analysis software (Image Pro Plus®) was used to extract intensity values from each image at every pixel along a line directly above the location of the thermocouples. Intensity values were extracted from corresponding Rhodamine B and Rhodamine 110 images and spreadsheet software (Excel) was used to produce the intensity ratios for each pixel along the line profile. A curve fit equation generated from calibration data was used to convert the intensity ratios into temperatures. Figure 3.2 shows the comparison between LIFT measured temperatures along a line profile with temperatures measured at a point by thermocouples at corresponding times.

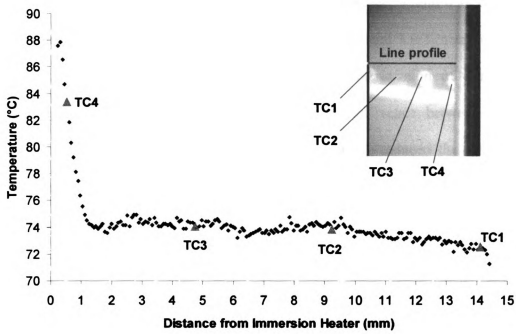

Figure 3.2: Comparison of thermocouple measurements with LIFT temperature measurements. Inset picture is a gray scale LIFT image showing the location of the thermocouples and approximate location of the line profile.

The inset picture is an unprocessed intensity image of the emission of Rhodamine B. The immersion heater is on the right side of the picture and the thermocouples are extending to the left. The intensity of each pixel along the line profile was divided by the corresponding pixel from the corresponding Rhodamine 110 intensity image. The location of the thermocouples was spatially resolved with the location of the line profile for direct comparison of the two temperature measurement methods. The maximum acquisition rate obtainable by the imaging equipment for this validation experiment was limited to approximately 0.5 Hz. The filter changer and the relatively long exposure times of 0.75s for each image limited the acquisition rate. This did not prove to be a problem for this experiment since the temperature of the fluid was changing at a rate close to 0.027°C/s. The data presented in Figure 3.2 show agreement between LIFT

and thermocouple temperature measurements to be, on average, within 0.88°C of each other. The maximum difference between thermocouples and LIFT occurred at the location closest to the immersion heater, which was the location of the steepest temperature gradient. At this point, the maximum difference between the two measurements was observed to be 1.5°C. Pixel averaging reduced the error in the region closest to the immersion and did not have much of an effect on the region farther away from the heater. This was probably due to the small gradients that existed away from the immersion heater. This test established confidence that LIFT can be used as an independent means for future measurements around radiofrequency probes when there is no other means to validate the LIFT measurements.

3.2 Image Acquisition Rate Improvement

The previous section indicated an imaging acquisition rate of 0.5 Hz. It is the goal of this thesis to obtain image acquisition rates close to 10 Hz. There are several things that can be done to improve acquisition rates. The first includes increasing the concentration of the fluorophores, which in turn increases the fluorescent emission intensity. This is effective up to a certain point. As the concentration of the fluorophores is increased, the optical clarity of the solution decreases making it more difficult to see a submerged heat source. A concentration of Rhodamine B between 0.05mg/l and 0.15mg/L is recommended. The ratio of concentrate between the two fluorophores was always kept at 20:1 so the amount of Rhodamine 110 recommended is 20 times less than that of Rhodamine B. This ratio was chosen based on work done by other researchers.[42] Figure 3.3 shows the effect concentration of the fluorophores has

on the measured emission intensity at a constant integration time. Integration times were chosen so that the measured intensity output of the lowest concentration was near 1000 counts out of 4096. A solution of 0.05mg/l Rhodamine B and 0.0025mg/l Rhodamine 110 was used as the starting point. The concentration of the solution was doubled and tripled and evaluated at the same integration times with the Ocean Optics spectrometer.

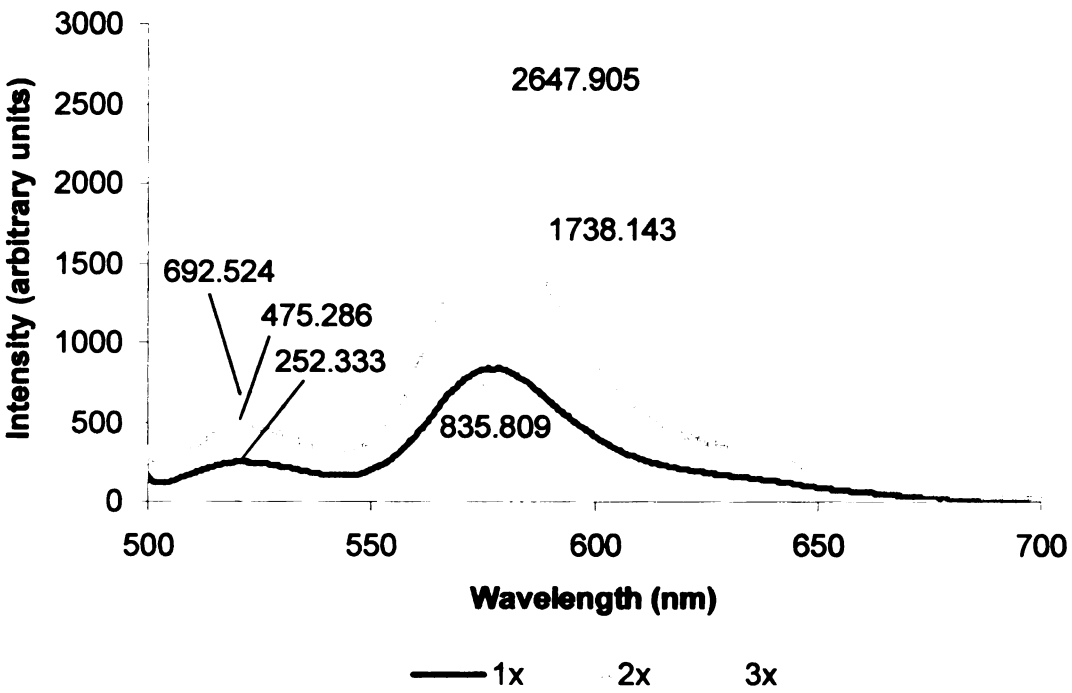

Figure 3.3: Effect of Concentration of Rhodamine B and Rhodamine 110 on Emission Intensity

Figure 3.3 indicates emission intensity values for the peak at 520nm (Rhodamine 110) and the peak at 576nm (Rhodamine B). These values essential increased in direct proportion to the fluorophore concentration. This suggests that the integration time can be reduced three fold by increasing the concentration of the solution from the 1x mixture to the 3x mixture. Since very small quantities of fluorescent chemical are being

mixed with relatively small volumes of fluid, an exact doubling or tripling was not expected with doubling or tripling the concentrate due to uncertainties in the measurement of the small quantities of fluorophore.

The intensity of the laser or power of the incandescent source used to excite the fluorescent solution can be increased in order to produce higher emission response from the fluorophores, thereby reducing the integration time needed by the detector to measure a signal. The downside to higher excitation intensities is that the fluorophores tend to quench at faster rates resulting in degradation of fluorescence intensity not resulting from a temperature change. Adrian[42] indicates that exposing a 3ml cuvette to a laser power of 0.5 W for duration of 120s results in negligible decay of fluorescence. The volume of fluid used for the experiments in this thesis was approximately 500ml, so it was concluded that the quenching effect of the laser at the same power setting was less than Adrian observed. Lasing of the fluorescent solution was limited to 120s and the power was never increased beyond 0.5W.

A third parameter that resulted in improved acquisition rate was the bin setting of the digital camera. The 0.5 Hz rate images were taken with no binning performed to the image. Binning reduces the resolution and amplifies the measured intensity. For example, a 2x2 bin will add the four nearest neighbor pixels together and replace the values of all four with the value of the sum. An image that was originally 1280 x 1024 pixels is reduced to an image of 640 x 514 pixels. The binning size used in this research was an 8 x 8 bin. This reduced the image to 160 x 128 pixels and provided a resolution of 90μm or 9 pixels per mm. This provided adequate resolution for the experiments.

The three parameters mentioned were controlled to provide the fastest integration times for the digital camera while maintaining adequate image resolution and optical clarity of the saline solution. The concentration of Rhodamine B was never increased above 0.045 mg/L and the laser power was kept at or below 0.5W, while binning did not exceed 8 x 8. The SensiCam digital camera was able to capture images at approximately 10 Hz mainly due to the 8 x 8 bin. This parameter had the most effect on integration speed and was the easiest parameter to adjust. The 8 x 8 binning made it possible to image with 10ms integration times. This would have produced a 100 Hz framing rate but this limit was reduced by the data transfer speed from the camera to the computer.

3.3 Field Temperature Measurements Around RF Probes

The LIFT method has been applied to quantify the temperature fields surrounding RF probes submerged in saline solution. The probes were held in the same fashion as illustrated in Figure 3.1 for the validation experiment with the immersion heater. Figure 3.4 shows an image of the radiofrequency probes and details of the probe tips. The monopolar probe on the left has a smooth tip surface and a 2.3mm diameter, whereas the bipolar probe on the right has a 3.0mm diameter and many holes evenly spaced in the tip. The reason for the holes is unknown. Initial tests with the LIFT method were conducted at framing rates near 1 Hz since the improvements in acquisition rate mentioned in the previous section were not yet implemented.

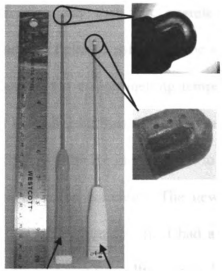

Monopolar Bipolar

Figure 3.4: Image of monopolar and bipolar radiofrequency probes. Close up images show the details of the probe tips.

For these experiments, the probe was operated in an optically clear tissue phantom gel. The characteristics of this gel are discussed below. A gel or solid medium was desired so that heat transfer would occur by conduction only, which would make it easier for eventual calculation of the heat flux from the probe tip. Another reason was to eliminate potential optical aberrations caused by convective flow currents and bubble formation resulting from the fluid medium de-gassing at high temperatures. De-gassing is the phenomenon witnessed before a fluid is brought to boil. As a fluid such as water is heated up, bubbles form on the surface of the container holding the fluid well before boiling occurs. This phenomenon was witnessed during the preliminary operations of the RF probes. In anticipation that the bubbles will obstruct the fluorescence emission intensity measurements, a gel phantom was created. The desired properties of the gel phantom are such that it is optically clear so that temperature can be measured within the medium. The gel must also be a good electrical conductor so that the RF probes

operate in the medium the same way that they operate in pure saline solution. Rhodamine B and Rhodamine 110 must be soluble in the medium. The last desired parameter is that the gel phantom has a high melting temperature greater than 90°C. However, this goal could not be realized at this time. The gel phantom was created by dissolving 30g/L gelatin (Sigma-Aldrich) in addition to the Rhodamine B and Rhodamine 110 fluorophores in saline solution. The new solution was a solid at temperatures less than 40°C. When in liquid form it had a higher viscosity than the saline solution. The gel medium was also optically clear as denoted by Figure 3.5. The probe can easily be seen as well as the camera lens on the other side of the glass test container. An important finding was that the addition of gelatin to the saline solution did not affect the calibration curves established in the previous chapter.

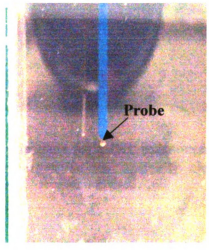

Figure 3.5: Image of monopolar RF Probe Submerged in an Optically Clear Gel Medium

Figure 3.6 is an image of the test equipment used for the LIFT experiments. The path of the Argon ion laser (Lexel Laser model 95) is denoted by the arrows. The laser beam is made into a sheet before impinging on the fluorescent medium containing

Rhodamine B and Rhodamine 110. The cylindrical lens, which transforms the laser beam into a sheet, is not observable in the image.

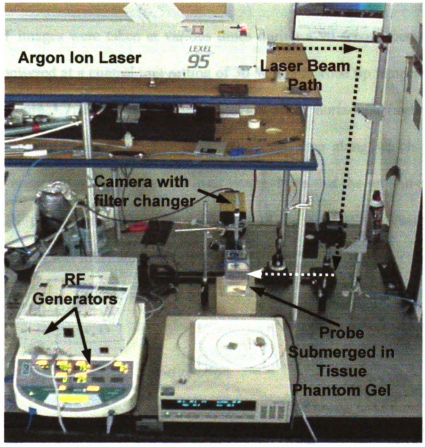

Figure 3.6: Experimental Equipment for LIFT measurements indicating the laser beam path, RF probe submerged in an optically clear tissue phantom, RF generators, and digital camera.

The bipolar RF generator, ArthroCare Corp., is on top and the monopolar RF generator, Oratec Interventions, is located on the bottom. The digital camera, Spectra Source Orbis, is located at the rear of the image. This camera was used in the preliminary studies but was switched to a newer camera with higher quantum efficiency, Cooke SensiCam, for experiments later in the research. The new camera made transient temperature analysis possible.

3.4 Results of LIFT measurement in gel medium

3.4.1 Monopolar

LIFT images were taken at various times during a 90 second period while the probe was powered at a control unit setting of 30 W and a probe tip temperature setting of 75°C. Figure 3.7 shows temperature variation along horizontal (x-direction) and vertical (y-direction) directions. The locations of the lines along which temperature profiles are measured are shown in the inset image. Note that the ground plate for the monopolar RF probe was mounted on the bottom of the test section directly below the tip of the probe as was illustrated in Figure 1.1.

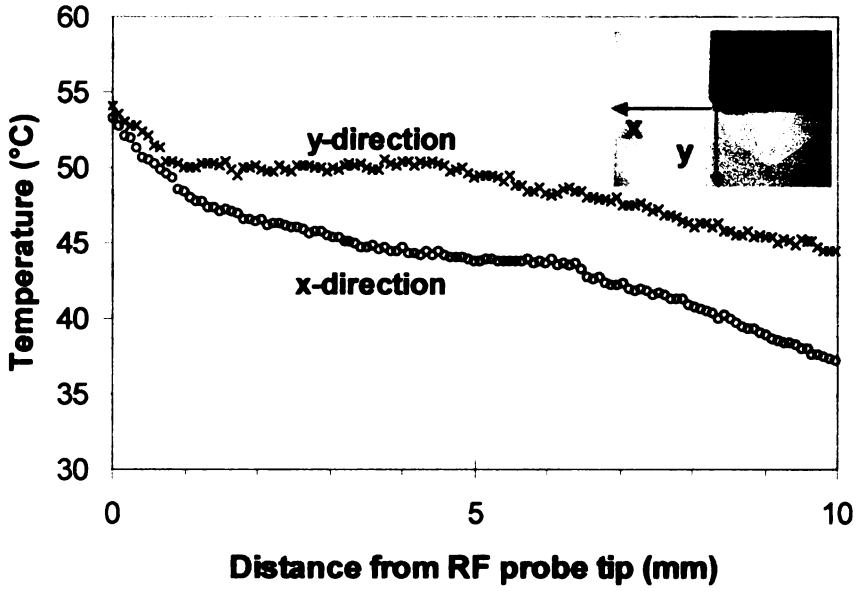

Figure 3.7: LIFT Predicted Temperature Around the Monopolar RF Probe

Before the experiments, it was not known whether the LIFT technique would produce reliable data near the probe tip due to the presence of small convection currents and the reflection of the laser light from the probe surface (both of these factors were believed

to have the potential to distort the LIFT measurements). It was observed during the experiments that the addition of gelatin to the solution served to reduce but not eliminate the convection currents. The laser light reflected from the probe surface also did not appear to be a major factor. For the monopolar RF probe, there were no observable optical aberrations in the image close to the probe tip. As seen in Figure 3.7, with a monopolar RF probe, a more pronounced thermal effect was observed in the vertical (y) direction than in the horizontal (x) direction. It is therefore obvious that the shapes of the isotherms around the probe are not symmetrical (for distances greater than 1mm).

3.4.2 Bipolar

Similar to the experiments performed with the Monopolar RF probe, LIFT images were taken at various times during a 90 second period while the probe was powered at a control unit setting of "1". The x-direction and y-direction line profile results from the bipolar RF probe are presented in Figure 3.8. Contrary to the monopolar probe examined, air bubbles formed very close to the tip of the bipolar RF probe, creating optical disturbances that affected the LIFT temperature measurements. The edge of the probe tip could not be distinguished clearly due to the aberrations. The size of the bubbles was less than 0.5 mm. Due to the presence of the bubbles, the data presented in Figure 3.8 are displaced away from the surface of the probe tip, beyond the location of the bubbles. When Figure 3.7 and Figure 3.8 are compared, it is observed that the temperature rise (in any direction) with the monopolar RF probe is greater than the bipolar. This observation is in very good agreement with published *in vitro*

experimental studies and numerical simulations [44]. The isotherms around the bipolar RF probe tip are more symmetrical than the monopolar case.

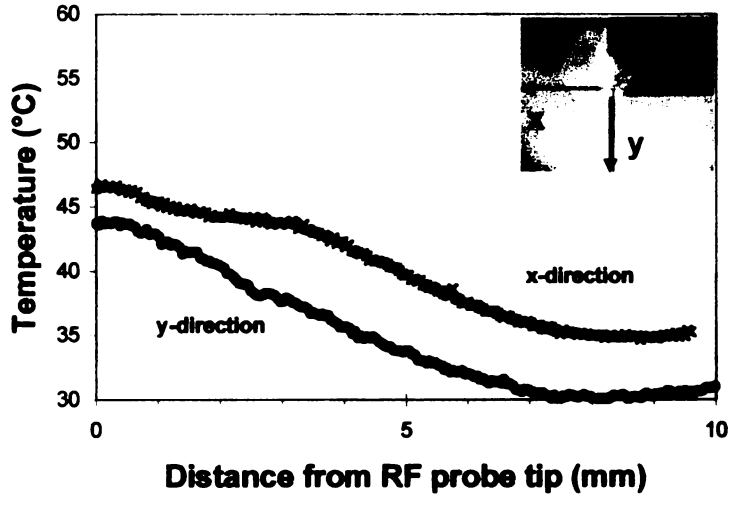

Figure 3.8: LIFT Predicted Temperature Around the Bipolar RF Probe

It was evident from the data that the bipolar probe created higher temperatures in the x-direction, whereas the monopolar probe created higher temperatures in the y-direction. This could be due to the location of the return electrode. For the monopolar RF case, the return electrode is placed under the tissue being heated. Therefore, the radiofrequency current flow from the probe tip through the tissue to the return electrode creates a volumetric heat generation within the target tissue. Due to these factors, it is reasonable to assume that the temperatures in the vertical direction will be higher, which is in agreement with the results presented here. Future experiments will be performed to test this hypothesis and to determine the effect that the location of the return electrode has on the temperature distribution in the surrounding medium.

The return electrode for the bipolar RF probe, as was illustrated in Figure 1.1, is located above the probe tip. Therefore, heat is generated in the saline or gelatin media

surrounding the probe tip and then is convected or conducted to the target tissue. It is essentially a surface heat transfer phenomenon. It is thus reasonable that the maximum temperature reached would be in the horizontal direction.

After these tests were conducted, an experimental design was established that more closely matched the actual operating conditions of the RF probes. Instead of using an entirely gel medium, a layer of gel was covered with saline solution. In this fashion, the gelatin layer represented a tissue phantom in which the probe was brought into light contact with the gelatin surface. Enough saline solution was added to submerge the probe tips to ensure proper operation of the RF probes. Figure 3.9 illustrates the configuration where the gel phantom is on the bottom with saline solution covering the phantom and submerging both RF probes in the fluid medium.

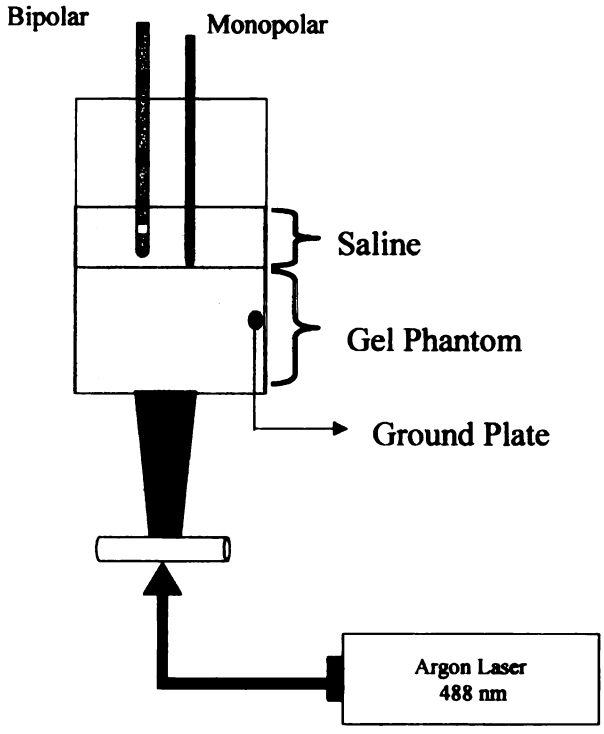

Figure 3.9: Gel phantom experimental configuration with the laser sheet passing through the bottom of the glass test container.

Both probes were not operated at the same time but are shown in the diagram to illustrate the relative distance the probes were operated from the gel surface. The saline solution and gel medium both contained Rhodamine B and Rhodamine 110 so that temperature in the both mediums could be measured. The laser sheet was brought through the bottom of the glass test container in order to illuminate both sides of the probe so that complete two-dimensional isotherms can be measured around the probe tip. The first setup brought the laser sheet in from the side so that the probe cast a shadow on one side of the probe, rendering LIFT useless in the shadowed region. The RF monopolar probe on the right is operated while in contact with the tissue phantom. For this experiment, the ground plate was mounted on the side of the test container instead of the bottom so that the laser sheet would be unobstructed. The bipolar RF probe on the left is operated 1 to 2mm from the surface of the tissue as described by surgeons who use the RF probes. The settings for both probes were kept the same as those used with the first experiments. The data acquisition speed was improved to 10Hz with the adjustment of the parameters mentioned beforehand. Instead of using the ratio of the intensity of Rhodamine B to the intensity of Rhodamine 110, only the intensity of Rhodamine B was used so that fast acquisition could be accomplished. If both images were taken, the framing rate would be reduced due to the time needed to switch the barrier filters in between image acquisitions. This single wavelength LIFT method was presented in Chapter 2 and proved accurate for relatively short time periods. The intensity of the laser proved to be very stable so intensity fluctuations due to variations in laser power were not evident but other optical aberrations do have the potential to disrupt the experiment.

Before testing began on the RF probes, the fluid and gel mediums were allowed to stabilize at room temperature and a thermocouple was used to measure the temperature of the fluid and gel medium. This temperature was used as the reference point when converting measured emission intensity into temperature. A reference Rhodamine B image was taken before the probe was turned on. Image acquisition was performed at 10 Hz for a time period of 120s. Matlab code was written to read each image and apply a regression analysis to each pixel in the image to covert measured emission intensities into temperatures. The Matlab code also produced movies in *.avi format. The code is presented in Appendix C.

The first probe evaluated was the monopolar probe. Figure 3.10 presents individual frames acquired during the test for a probe set point of 30W, 75°C. The color scale on the right side of the images ranges from 20°C to 80°C. Image A was acquired 1 to 2 seconds after the probe was activated. Note the vortices rising along the probe sides. These convective currents were characteristic of the monopolar measurements shortly after activation. Image B was acquired after 45s of probe activation. Temperatures in the gel reached nearly 60°C and all temperatures higher than 40°C were assumed to be regions of liquid gelatin. The monopolar RF probe produced symmetric isotherms with more thermal penetration in the vertical direction than in the horizontal direction. These results are in agreement with the results presented earlier in Figure 3.7.

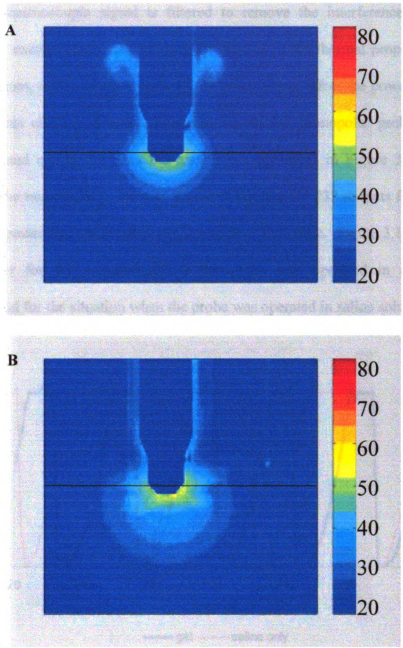

Figure 3.10: Whole field temperature measurement in a gel and saline medium due to monopolar RF heating. Line indicates gel-saline interface. Image A is 1 to 2 seconds post activation and image B is 45 seconds post activation.

A direct comparison between the two tests was not made since the operating mediums were different for the two tests. The monopolar probe has a T-type thermocouple embedded in the stainless steel tip, which is used as a reference for power control of the

probe. The thermocouple signal is filtered to remove the interference caused by radiofrequency energy. It is assumed that differences in the thermal properties of the operating medium, or the size and mass of the target object affect the power control of the probe. This effect was tested by operating the RF monopolar probe in saline solution only and comparing it to the results just presented in Figure 3.10. A RF generator for the monopolar probe was acquired that had RS 232 outputs for computer acquisition of power and temperature performance of the probe. Figure 3.11 shows the reported power for the situation where the probe was operated in a gel-saline environment and for the situation when the probe was operated in saline solution only.

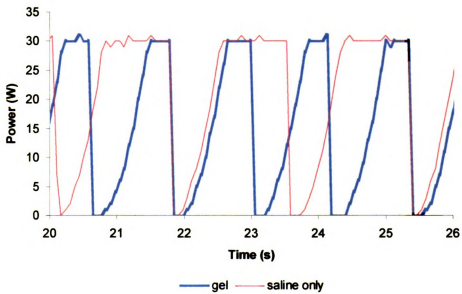

Figure 3.11: Measured power output for the RF monopolar probe in a gel-saline medium and in a saline solution only medium.

The results in Figure 3.11 indicate that the saline solution environment required more "on time" than that of the gel-saline medium. A probable cause for this is that the probe

needs to stay powered longer for the saline solution medium since heat is transported away from the probe tip more than when the gel medium is present.

The same procedure was followed for temperature measurements around the bipolar radiofrequency probe at a set point of '1'. The results are presented in Figure 3.12 for 1 to 2 seconds post activation (image A) and for 100s post activation (image B). The line represents the gelatin-saline solution interface, which was approximately 2mm below the bipolar probe tip. The arrows in image B indicate bubble formation. The bipolar probe was plagued with the formation of bubbles much more than the monopolar probe tip. The two probes were operated at comparable settings so one probe was not experiencing much higher temperatures than the other one.

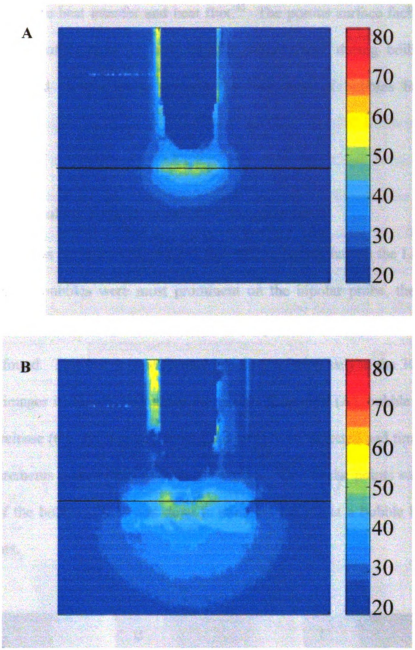

Figure 3.12: Whole field temperature measurement in a gel and saline medium due to bipolar RF heating. Line indicates gel-saline interface. Image A is 1 to 2 seconds post activation and image B is 100 seconds post activation. Arrows in image B indicate bubbles.

A possible reason for the bubble formation might be due to the contours of the probe tip. The bipolar probe has many holes located on the probe tip and in general is not as smooth as the monopolar probe. Rough surfaces and surfaces with small cavities are

reported to enhance heat transfer and heat flux.[45] The porous surface facilitates vapor formation and is often used for heat transfer enhancement during boiling. A gel medium was used to attempt to remove the formation of bubbles but this was unsuccessful.

3.4.3 Effect of Bubble Formation on LIFT Measurements

A study was performed to quantify the effect a bubble has on the LIFT method. Even though the bubbles were most prominent on the bipolar probe, the monopolar probe was used as an example since a clear example of bubble formation to bubble release was found. This test was performed in saline solution only at the 30W 75°C set point. The images in Figure 3.13 show the bubble formation (A), bubble growth (B), and bubble release (C). Four points around the probe were selected and time dependent LIFT measurements were extracted from the images. One of the points was located at the center of the bubble. This was done to examine the effect a bubble has on LIFT measurements.

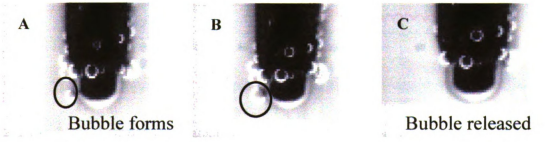

Figure 3.13: Bubble formation on RF monopolar probe tip. Bubbles create an optical disturbance that effects LIFT measurement.

Figure 3.14 shows the time dependent LIFT measurements at the five locations indicated on the inset picture. The closest points were within 1mm of the probe tip whereas the furthest point was approximately 3mm from the probe tip. The data show temperatures cycling at approximately 1 Hz between 30° and 40°C at the points closest to the probe tip. The point furthest away from the probe fluctuated between 25°C and 30°C. The temperature data from the monopolar probe unit are also plotted and represented as the point on the probe tip. The data measured by LIFT and that measured by the RF control unit agreed with each other with respect to the frequency of temperature cycling. This indicates that the LIFT method can track 1 Hz temperature fluctuations over a 10°C/s heating and cooling rate.

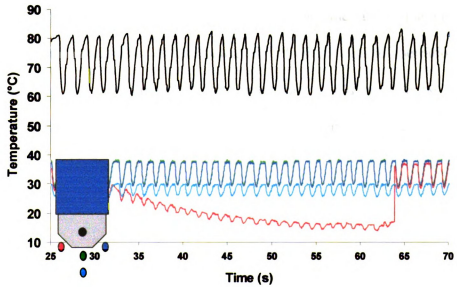

Figure 3.14: Temperature measurement effect of bubble formation. The points around the probe tip represent the relative location of the measurements.

The data at the location of the bubble show an apparent temperature decrease as the bubble is formed and a temperature measurement restoration once the bubble is released. The formation of bubbles can potentially cause a temperature error in either direction because the spherical geometry of the bubble can decrease the fluorescence intensity resulting in a measured temperature increase or intensify the fluorescence resulting in a measured temperature decrease. The LIFT measurement was still able to track the temperature fluctuation rate through the bubble indicating that it may be possible to correct the error by using the corresponding intensity signal from the Rhodamine 110 fluorophore. The Rhodamine 110 intensity signal was not measured for this experiment since fast acquisition rates were desired. It is assumed the bubble would cause a corresponding decay or increase in fluorescent intensity signal for the Rhodamine 110 fluorophore. If this proves to be true, then the ratio of the intensities of Rhodamine B and Rhodamine 110 can potentially eliminate optical aberrations caused by the bubbles. The measurement of the intensities would need to be performed "simultaneously". Two cameras optically focused on the same region of interest is one method to attempt this correction.

3.5 FERIT Measurements on the Monopolar RF Probe

The FERIT method was applied to measure temperatures on the surface of the monopolar probe tip for a probe set point of 30W 75°C. This method was only applied to the monopolar probe since the bubble formation on the tip of the monopolar probe was significantly less than the bipolar probe. Future tests will include measurements on the bipolar probe once an effective method has been established to handle the added

challenge of imaging through bubbles. The ratiometric method presented in Chapter 2 using a single reference image was applied. Prior to the actual test, the probe coated with the Europium polymer was calibrated in the glass test chamber by incrementally increasing the temperature of the fluid in the test vessel and taking images when isothermal conditions were realized as judged by thermocouple measurements in the fluid medium. The thermocouple in the probe tip was also utilized during the calibration procedure for reference. Images were acquired at 10Hz while the probe was powered. A Matlab program similar to that used in the LIFT measurements converted fluorescence intensity into temperature (details in Appendix C). Figure 3.15 presents 2 sequential images in time showing the probe increasing in temperature during one of its power cycles. The temperature scale for the images was 20°C to 90°C.

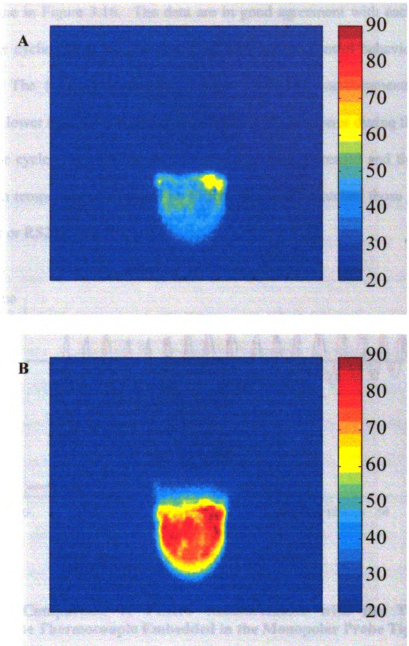

Figure 3.15: FERIT Measurements on the Surface the Monopolar Probe Tip

The results obtained with FERIT were compared to the data output from the RF generator. This comparison was made by extracting temperature data averaged over a 3 x 3 pixel area at the center of the probe tip for each FERIT image and plotted with

respect to time in Figure 3.16. The data are in good agreement with each other with respect to the cyclic power on and power off temperature control behavior of the RF generator. The first eight seconds showed the FERIT measurements measuring temperatures lower than the output temperature from the generator during the power off portion of the cycle. This difference diminished as time increased and the maximum and minimum temperatures measured by FERIT eventually matched those produced by the generator or RS232 data.

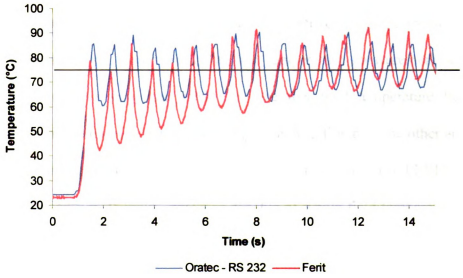

Figure 3.16: Comparison of FERIT Measurements with the Temperature Measured by the Thermocouple Embedded in the Monopolar Probe Tip

The line drawn on the plot in Figure 3.16 represents the set point of 75°C entered on the control panel of the RF generator. The data show that the generator maintained an average of approximately 75°C by cycling the temperature between 60°C and 85°C. The temperatures measured by LIFT in the saline solution at locations within 1mm of the probe tip indicated oscillating temperatures ranging from 30°C to 40°C. This suggests convection quickly removes the heat generated by the RF probes.

Chapter 4: Conclusions and Future Work

The majority of the work for this research was spent testing fluorescent chemicals in order to understand their temperature dependent fluorescence characteristics and using the techniques developed performing measurements on radiofrequency heating devices and for applications where cryogenic temperatures are present. The next step would be to use the temperature measurement techniques developed in order to study the effect that the measured temperature has on its surrounding environment whether it is a biological application or some other area where conventional temperature measurement methods are not suitable. The FERIT and LIFT methods are the only methods in existence capable of whole field temperature analysis within a fluid medium or on a surface submerged in a fluid and for whole field analysis at cryogenic temperatures. This benefit alone opens the door to perform detailed experiments on everything related to cryobiology and to radiofrequency heating.

The results presented in the previous chapters showed the LIFT and FERIT method could be used to make temperature measurements at an acquisition rate of 10 Hz, with a maximum error of 1.5°C, and with 90 μm spatial resolution. This spatial resolution is limited by the optics used. The fundamental limit is the wavelength of visible light, which is on the order of 0.5μm. The LIFT method, which was previously developed by other researchers for measurements from 24°C to 40°C, has been

extended to measure temperatures as high as 90°C. The FERIT method previously developed under the supervision of the principal investigator has been extended from a range of 24°C to 80°C down to –80°C.

Accuracy can be improved by implementing a dual camera system so that both emission spectra can be measured for the LIFT method. The FERIT method can benefit from this too by possibly combining Europium with another fluorescent chemical that may be temperature invariant.

Fluorescent thermography methods offer many benefits over conventional temperature measurement techniques and at the same time are not appropriate to use for certain situations. Implementing a fluorescence thermography system is not an easy endeavor and the benefits of the method should definitely outweigh the time required to learn the method. Fluorescence thermography has been compared to some other conventional methods in Table 4.1. Thermocouples, fluoroptic thermometry, infrared thermometry are all relatively easy methods to implement. Someone new to those methods can make accurate measurements in less than 1 day. However, fluorescent thermography methods require months for someone who has little knowledge of the method. The most time consuming part is to establish confidence in the calibration so that the user will have assurance the results are accurate when actual measurements are made independent of other conventional methods.

Fluorescent thermography methods are limited by acquisition speed since the fluorescent emission signal from the fluorophore is sometimes weak, requiring long integration times by sensitive digital cameras. The digital cameras are also limited by the data transfer rate to the computer. The performance of the digital cameras is

expected to improve with time so the acquisition rates will continue to improve with technology advancement. In order achieve 10 Hz framing rates, binning was performed on the image, thereby reducing the spatial resolution. Acquisition speed will also improve as cameras become more sensitive to low intensity light.

The limitations of the other temperature measurement methods are the situations that make fluorescence thermography appealing. Fluorescence thermography is limited by the equipment necessary for application since it requires several components. This will make application of fluorescence thermography in a confined space difficult. Another limitation of fluorescence thermography is the cost.

	Level of Difficulty:	Acquisition Speed:	Accuracy:	Temp. Range:	Spatial Resolution:	Limitations:
Thermocouple	Low	High	1-2°C	-240°C to 2300°C	Low (NA)	RF fields, Corrosive chemicals
Fluoroptic Thermometry	Low	Low (4 Hz)	1°C	-200°C to +450°C	Low (NA)	Size of probes, Acq. speed
Infrared Thermography	Moderate	Moderate to High (8Hz – 60Hz)	1°C	-40°C to +2000°C	High (10 μm)	Opaque to fluids, Low end temp
Fluorescent Thermography	High	Moderate (10 Hz +)	1.5°C	-170°C to 2000°C	High (0.5 μm)	multi-component

Table 4.1: Comparison of conventional temperature measurement methods with fluorescent temperature measurements.

Current cost of the LIFT experimental equipment was $55,000. If dual camera measurements are desired, another $15,000 should be added to the cost. This is cheaper than some IR thermography units that can cost over $100,000.

4.1 Future Developments for Application of LIFT and FERIT to RF Heating

The development of the LIFT technique makes it possible to explore the effect many variables have on the outcome of thermal therapies applied to biological material. In clinical applications, saline solution is circulated in the cavity where the target tissue is being treated to avoid the formation of hotspots and to wash away debris. Future tests include circulating the saline around the probe tip at different flow rates to determine the best rate that prevents overheating of the tissue. In addition to flow rate, probe sweep speed is a deciding factor that determines the amount of heat transferred into the material being treated. Presently surgeons operate the probe in a manner that they perceive to be visually effective. Quantifying the effects of this parameter will enable surgeons to perform more effectively by defining probe velocities that may be detrimental to the patient. A test configuration similar to the gel medium covered with saline can be used in conjunction with a mechanical arm that sweeps the probe over the tissue phantom surface. The depth of thermal penetration can then be quantified with probe sweep speed as well as with the RF control unit settings.

Beyond the clinical applications, developers of RF probe units can verify if their control parameters are producing the desired temperature fields. Currently RF probe manufacturers lack the thermal detail measured in this thesis.

A recent attempt was made to perform LIFT and FERIT simultaneously during an experiment. This would make it possible to directly measure the heat flux from probe tip into the heated medium. Problems arose trying to keep the emission spectra of Rhodamine B and Europium separate. Nonetheless this possibility should be explored in the future.

The combination of data provided by the LIFT and FERIT methods should enable accurate boundary conditions to be determined for finite element simulations (FEM). Finite element models can even be set up to simulate the tissue phantom experiments. If good agreement between experiments and FEM can be obtained, then the material properties in the model could be changed to represent biological material with the assumption that the FEM model is accurate based on the validation with the tissue phantom experiments.

4.2 Future Application for the Low Temperature FERIT Method

A future application of the cryogenic FERIT method is to apply the polymer film to the glass window located in the dorsal skin flap chamber and monitor temperatures on the surface while conducting cryosurgery. Figure 4.1 shows a sketch of the dorsal skin flap chamber. The image to the right is an image of the cancer cells inside the window chamber. The cancer cells have been genetically marked with green fluorescent protein (GFP), tagging them as bright green spots in the inset image. Blood vessels are also visible in the window chamber as dark channels. If detailed temperature measurements were made on the glass window surface using the FERIT

method and Terbium during cryosurgery, these measurements could be used to correlate temperature to the type of tissue damage observed beneath the window chamber. The cancer cells can be destroyed either by rapid freezing rates, which cause the cells to burst, or by destroying the blood vessels nearby the cancer cell clusters, which will starve the cells.

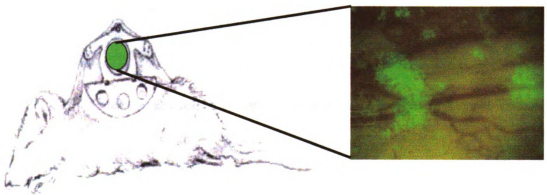

Figure 4.1: Potential application of low temperature FERIT to measure temperatures on the window chamber during cryosurgery in order to correlate temperature and thermal damage.

The polymer coating should also be semitransparent so that the cells and blood vessels can be observed with a microscope. Since IR cameras cannot measure temperatures down to cryogenic levels and thermocouples are invasive, the FERIT method could lead to great advancements for correlating temperature and cooling rates to cellular death and vascular injury.

The intended use of GFP is as a marker for cell viability. If a cell dies so does the fluorescence associated with the GFP. During cryosurgeries the fluorescence intensity of the tumor was observed to increase as the freezing protocol was applied to the tissue in the window chamber. Figure 4.2 illustrates the qualitative increase in

fluorescence intensity as the cancer cells are frozen, and a decrease in fluorescence as the cells return to their normal temperature.

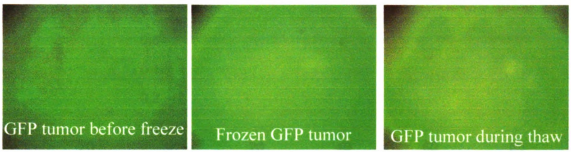

Figure 4.2: GFP Tumor Qualitative Intensity Measurements During Freeze-Thaw Cycle

A pilot test was conducted to evaluate the temperature dependence of the fluorescence intensity of GFP. Pure GFP was placed in a cuvette in the spectrometer sample folder and analyzed from –12°C to 60°C. The 488nm light source used to evaluate the Rhodamine B and Rhodamine 110 solutions was used to excite the GFP solution. The temperature of the solution was decreased as low as the Neslab bath could obtain. The results presented in Figure 4.3 show that GFP exhibits temperature dependence from -12°C to 60°C. Further experimentation needs to be conducted to determine the entire temperature dependent fluorescence range of GFP. GFP has the potential to be an effective cellular temperature indicator.

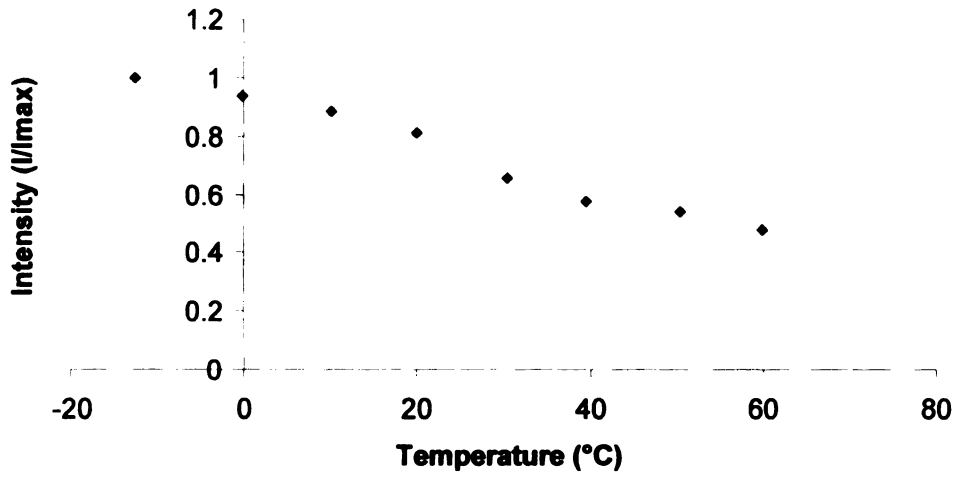

Figure 4.3: Temperature dependent fluorescence of GFP from –12°C to 60°C.

Appendix A: Procedure for Terbium and Europium Preparation

Chemical Preparation:

Terbium (III) Chloride hexahydrate and Europium (III) Chloride hexahydrate must be chemically altered before being used as a temperature dependent fluorophore. The chemicals appear as a "salt" in their unprocessed form and do not exhibit any fluorescent characteristics.

1. Mix 0.587 grams of Europium (III) Chloride or 0.598 grams of Terbium (III) chloride in 50ml of distilled or deionized water.
2. Increase the pH of the solution to approximately 8.5 by adding ammonium hydroxide. The solution should thicken as the pH is increased.
3. While stirring add 1 gram of hexafluoroacetylacetone (hfa) to the mixture. Crystals should form immediately.
4. Empty the liquid and fluorescent crystals into a shallow container with a large bottom surface and place on the heater table for a setting of '1' (70°C).
5. Allow the liquid to evaporate in a fume hood and thoroughly dry the crystals (approximately 2hrs).
6. Using a razor blade, scrape the dried fluorescent precipitate off the bottom and sides of the container and store in an appropriate container.

Fluorescent Paint Preparation:

The following is the procedure to prepare the fluorescent precipitate made in the previous steps for application.

1. Weigh 10g of Methyl Ethyl Ketone (MEK) in a medium sized airbrush spray bottle.
2. Add 0.15g of fine PMMA pellets to the MEK.
3. Place a magnetic stir bar in the bottle and cover the bottle with aluminum foil.
4. Place the jar on the heat/stir table and set the heater at position '1' (70°C) while stirring the solution.
5. Heat and stir the solution for about 30min or until the PMMA can no longer be seen.
6. Turn off the heater and allow the solution to cool to room temperature while stirring.
7. Weigh 0.05g of the fluorophore (Europium or Terbium) and mix the solution.
8. Connect the bottle to the airbrush and adjust the flow of air as needed.
9. Apply a fine coat to the test surface and allow the liquid to evaporate. Care should be taken not to over spray the surface since this will produce a non-uniform polymer film.
10. Illuminate the sample with a handheld UV source to check the uniformity and concentration of the fluorophore.

11. Reapply coats as necessary until the desired effect is obtained. The polymer film will not be evident to the eye.

12. Apply gentle heat to the coated surface to evaporate the MEK and 'set' the polymer film. The film goes from transparent to a fine white frosting.

Appendix B: Light Source Evaluation with Ocean Optics Spectrometer

Evaluation of the spectral output of the light sources used in this thesis was accomplished with the Ocean Optics Spectrometer. A 3mm diameter fiber optic cable (black), not originally included with the spectrometer system, was used to direct the light output by the individual light sources into the spectrometer sample holder without a sample present. The size of this fiber optic required removing the light collimator screwed into the sample holder. A 600μm diameter fiber optic (blue) included with the spectrometer system was mounted 180° from the 3mm fiber. The opposite end of this fiber was connected to the spectrometer. The other end of the 3mm fiber was held by hand in front of the light source being evaluated until the spectrometer recorded the spectral emission. Integration times were on the order of 10ms for all the light sources evaluated. Neutral density filters were placed in the filter slot located in the sample holder in between the two fibers as needed to prevent the spectrometer from becoming saturated due to the high intensities of the light sources. Typically, three low transmissivity filters were needed to reduce the intensity of the light sources to a measurable level. The evaluation of the light sources is presented in Figure B 2.

The Opti Quip light source is a high intensity Xenon source that produces electromagnetic emission peaks at 365nm, 408nm, 439nm, 548nm, and 580nm. Bandpass filters can be used to single out a particular peak for excitation of fluorescent samples. A 365nm bandpass filter was mounted to the Opti Quip source for evaluation of the FERIT fluorophores. The evaluation of this configuration is denoted as "Opti w/UV" in Figure B 2.

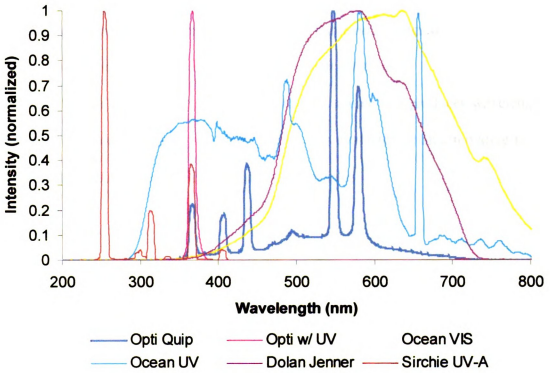

Figure B 2: Evaluation of the Spectral Emission of Electromagnetic Excitation Sources with the Ocean Optics Spectrometer

The addition of the bandpass filter eliminated the other emission peaks included in the original source.

The Ocean Optics visible and UV emission spectra are included in Figure B 2 and was discussed in the main part of the thesis. It should be noted that this source is not as intense as the other sources evaluated. Integration times on the order of 60s were necessary when using this source to evaluate Rhodamine B fluorescent samples. This led to the use of the Dolan Jenner source, which reduced integration times to 10s for the same fluorophore concentration.

The Dolan Jenner source emits over the whole visible spectra with peak emission near 600nm. However, a 488nm, 10nm bandwidth, filter was used with this source to excite the Rhodamine B and Rhodamine 110 solutions.

The Sirchie UV-A source is a hand held light source that produces wavelengths in the short UV wavelength region. This source was evaluated as an alternative to the Opti Quip source to excite the FERIT fluorescent samples.

Appendix C: Matlab Code for FERIT and LIFT Whole Field Analysis and AVI Creation

The following Matlab codes convert gray-scale intensity images in tiff sequence format obtained with the SensiCam digital camera and Image Pro Plus software into a pseudo colored temperature avi file. The LIFT and FERIT code differ in the equations used to convert gray scale intensity ratios into temperatures. Besides that the codes are relatively similar. These codes produced the images in Figure 3.10, Figure 3.12, and Figure 3.15. The avi files produced by these codes are very large and should be converted to mpeg format before using in a presentation.

LIFT Code:

```
clear all
Ref = imread('ORgelref.tif');
i=1;
y=1;
sumb=0;
for i=1:5
   B = imread('ORgelseq.tif',i);
   sumb=double(B)+sumb;
end
Bref=sumb./5;
normalizer = double(Bref)./double(Ref);
i=6;
while i<=995
   B = imread('ORgelseq.tif',i);
   ratio=double(B)./double(Ref)./normalizer;
   temperature=-858.46.*ratio.^5+2934.2.*ratio.^4-3920.6.*ratio.^3+2607.3.*ratio.^2-
951.85.*ratio+212.38;
   imagesc(temperature,[20 80]); colormap(jet(15));
   title('Oratec Monopolar Probe with Gel (30W, 75C set point)');
   set(gca,'XTicklabel',{},'YTicklabel',{});
   colorbar('vert');
   tempmap(y) = getframe(gcf);
   i=i+2;
   y=y+1;
end
```

```
movie2avi(tempmap,'ORgel.avi','quality', 100,'fps',15)
```

FERIT Code:

```
clear all
i=1;
y=1;
sumb=0;
for i=1:1
   B = imread('sp2seq.tif',i);
   sumb=double(B)+sumb;
end
normalizer = sumb./1;
i=6;
while i<=50
   B = imread('sp2seq.tif',i);
   ratio=double(B)./normalizer;
   temperature=107.241315030887+8.23585848058315.*ratio-
848.008378147134.*ratio.^2+2358.20293067844.*ratio.^3-
2590.20299792734.*ratio.^4+987.5232610519.*ratio.^5;
   imagesc(temperature,[20 90]); colormap(jet(20));
   title('ArthroCare Bipolar Probe, (set point 2)');
   set(gca,'XTicklabel',{},'YTicklabel',{});
   colorbar('vert');
   tempmap(y) = getframe(gcf);
   i=i+1;
   y=y+1;
end
movie2avi(tempmap,'feritAC.avi','quality', 100,'fps',15)
```

BIBLIOGRAPHY

[1] Neubert, P.,US Patent No. 2,071,471 (1937).

[2] Arnoczky, S.P., Aksan, A., 2001, " Thermal Modification of Connective Tissues: Basic Science Considerations and Clinical Implications," *American Academy of Orthopaedic Surgeons Instructional Course Lectures*, Sims, F.H. (ed.), AAOS, Chicago, IL, **50**, pp.3-11.

[3] Anderson, K., McCarty, E.C., and Warren, R.F., 1999, "Thermal Capsulorrhaphy: Where Are We Today," Sports Medicine and Arthroscopy Review, **7**, pp. 117-127.

[4] Perry, J.J., Higgins, L.D., 2000, "Anterior and Posterior Cruciate Ligament Rupture After Thermal Treatment," Arthroscopy, **16**, 7, pp. 732-736.

[5] Derby, R., et al., 2000, "Intradiscal Electrothermal Annuloplasty (IDET): A Novel Approach for Treating Chronic Discogenic Back Pain," Neuromodulation, **3**, 2, pp. 82-88.

[6] Saal, J.S., Saal, J.A., 2000, "Management of Chronic Discogenic Low Back Pain with a Thermal Intradiscal Catheter - A Preliminary Report," Spine, **25**, 3, pp. 382-388.

[7] Cilesiz, I., Thomsen, S., Welch, A.J., 1997, "Controlled Temperature Tissue Fusion: Argon Laser Welding of Rat Intestine In Vivo, Part One," Lasers in Surgery and Medicine, **21**, pp. 269-277.

[8] Brinkmann, R., et al., 2000, "Influence of Temperature and Time on Thermally Induced Forces in Corneal Collagen and The Effect on Laser Thermokeratoplasty," Journal Of Cataract and Refractive Surgery, **26**, 5, pp. 744-754.

[9] Kampmeier, J., et al., 2000, "Thermal and Biomechanical Parameters of Porcine Cornea," Cornea, **19**, 3, pp. 355-363.

[10] Edwards, R.B., et al., 2002, "Thermal Chondroplasty of Chondromalacic Human Cartilage - An Ex Vivo Comparison of Bipolar and Monopolar Radiofrequency Devices," American Journal of Sports Medicine, **30**, 1, pp. 90-97.

[11] Shellock, F.G., Shields, C.L., 2000, "Radiofrequency energy-induced heating of bovine articular cartilage using a bipolar radiofrequency electrode," American Journal of Sports Medicine, **28**, 5, pp. 720-724.

[12] Kuo, T., et al., 1998, "Collagen Thermal Damage and Collagen Synthesis After Cutaneous Laser Resurfacing," Lasers in Surgery and Medicine, **23**, pp. 66-71.

[13] Fitzpatrick, R.E., et al., 1996, "Pulsed Carbon Dioxide Laser Resurfacing of Photoaged Facial Skin," Archives of Dermatology, **132**, pp. 395-402.

[14] Naseef III, G.S., et al., 1997, "The Thermal Properties of Bovine Joint Capsule," American Journal of Sports Medicine, **25**, 5, pp. 670-674.

[15] Hayashi, K., et al., 1996, "The Effect of Nonablative Laser Energy on the Ultrastructure of Joint Capsular Collagen," Arthroscopy, **12**, 4, pp. 474-481.

[16] Allain, J.C., et al., 1980, "Isometric Tensions Developed During the Hydrothermal Swelling of Rat Skin," Connective Tissue Research, **7**, pp. 127-133.

[17] Miles, C.A., et al., 1995, "The Kinetics of the Thermal Denaturation of Collagen in Unrestrained Rat Tail Tendon Determined by Differential Scanning Calorimetry," Journal of Molecular Biology, **245**, pp. 437-446.

[18] Cilesiz, I., et al., 1997, "Controlled Temperature Tissue Fusion: Argon Laser Welding of Rat Intestine In Vivo, Part One," Lasers in Surgery & Medicine, **21**, pp. 269-277.

[19] Pearce, J.A., et al., 1993, "Kinetics for Birefringence Changes in Thermally Coagulated Rat Skin Collagen," Proceedings of SPIE, **1876**, pp. 180-186.

[20] Le Lous, M., et al., 1983, "Hydrothermal Isometric Tension Curves from Different Connective Tissues. Role of Collagen Genetic Types and Noncollagenous Components," Connective Tissue Research, **11**, pp. 199-206.

[21] Kang, T., et al., 1995, "Heat-Induced Changes in the Mechanical Properties of Passive Coronary Arteries," Journal of Biomechanical Engineering, **117**, pp. 86-93.

[22] Privalov, P.L., 1982, "Stability of Proteins - Proteins Which do not Present a Single Cooperative System," Advances in Protein Chemistry, **35**, pp.1-104.

[23] Tang, J., et al., 1997, "Morphologic Changes in Collagen Fibers After 830 nm Diode Laser Welding," Lasers in Surgery and Medicine, **21**, pp. 438-443.

[24] Privalov, P.L., 1989, "Thermodynamic Problems of Protein Structure," Annual Reviews in Biophysics and Chemistry, **18**, pp.47-69.

[25] Olde Damink, L.H.H., et al., 1995, "Glutaraldehyde as a Crosslinking Agent for Collagen-Based Biomaterials," Journal of Materials Science: Materials in Medicine, **6**, pp. 460-472.

[26] LeCarpentier, G.L., 1993, "Continuous Wave Laser Ablation of Tissue: Analysis of Thermal and Mechanical Events," IEEE Transactions on Biomedical Engineering, **40**, 2, pp. 188-199.

[27] Omega Engineering, http://www.omega.com/techref/, 2002

[28] Luxtron Corporation, http://www.luxtron.com, 2002

[29] FLIR, http://www.flirthermography.com/, 2002

[30] Modest, M., F., Radiative Heat Transfer, McGraw Hill, Inc. 1993.

[31] Lakowicz, J., R., Principles of Fluorescence Spectroscopy, (1999), Kluwer Academic/Plenum Publishers, New York.

[32] Allison, S., W., Gillies, G., T., "Remote Thermometry with Thermographic Phosphors: Instrumentation and Applications," Rev. Sci. Instrum. 68 (7), July 1997. pp 2615-2650.

[33] Rayleigh and Raman Scattering, Fluorescence and Phosphorescence, web reference.

[34] Edwards, D.,K., Radiation Heat Transfer Notes

[35] Engler, R.H., et al., "Pressure Sensitive Paint Systems for Pressure Distribution Measurements in Wind Tunnels and Turbomachines," Meas. Sci. Technol. (11), 2000. pp. 1077-1085.

[36] Allison,S.,W., Cates, M.R., Beshears, D.L., "A Survey of Thermally Sensitive Phosphors for Pressure Sensitive Paint Applications," Oak Ridge National Laboratory.

[37] Lian, Bin, "Fluorescent Emission Ratio Imaging Thermography and its Application in Heat Transfer Analysis," Ph.D. Thesis, MSU, 1999.

[38] Edge, A.C., Laufer, G., Krauss, R.H., "Surface Temperature -Field Imaging with Laser-Induced Thermographic Phosphorescence," Applied Optics, vol.39, no. 4, Feb 2000. pp. 546-553.

[39] Bhaumik, M.L., "Quenching and Temperature Dependence of Fluorescence in Rare-Earth Chelates," the Journal of Chemical Physics, 10, (12), June 1964. pp. 3711-3715.

[40] Ananias, Duarte, et al., "Novel Microporous Europium and terbium Silicates," J. Am. Chem. Soc., 2001, 123, 5735-5742.

[41] Ranson, R.M., Thomas, C.B., Craven, M.R., "A Thin Film Coating for Phosphor Thermography," Meas. Sci. Technol. 9 (1998). pp. 1947-1950.

[42] Sakakibara, J., Adrian, R.J., "Whole Field Measurement of Temperature in Water Using Two-Color Laser Induced Fluorescence," Experiments in Fluids 26 (1999). pp. 7-15

[43] Kim, H.J., Kihm, K.D., "Application of a Two-Color Laser Induced Fluorescence (LIF) Technique for Temperature Mapping," 2001 ASME Internation Mechanical Engineering Congress and Exposition.

[44] Aksan, A., Nielubowicz, D.S., McGrath, J.J., 2001 "Modeling The Thermal Histories Of Collagenous Tissues Subject To Different Heating Modalities," HTD-24433, *Proceedings of ASME Winter Annual Meeting.*

[45] Cengel, Yunus, Heat Transfer, a Practical Approach, (1998), McGraw Hill, Boston, Mass.